Published in Journal of Optics A: Pure and Applied Optics 8, issue 7, 407-429, 2006
which should be used for any reference to this work

Comparing glass and plastic refractive microlenses fabricated with different technologies

H Ottevaere[1], R Cox[2], H P Herzig[3], T Miyashita[4], K Naessens[5], M Taghizadeh[6], R Völkel[7], H J Woo[8] and H Thienpont[1]

[1] Department of Applied Physics and Photonics (TONA-IR), Vrije Universiteit Brussel, Pleinlaan 2, B-1050 Brussel, Belgium
[2] MicroFab Technologies, Inc., 1104 Summit Avenue, Suite 110, Plano, TX 75074, USA
[3] Institute of Microtechnology, University of Neuchâtel, Rue A-L Breguet 2, CH-2000 Neuchâtel, Switzerland
[4] Ricoh Company Ltd, Research and Development Group, 3-2-3, Shin-Yokohama, Kohoku-ku, 222-8530 Yokohama-shi, Japan
[5] Department of Information Technology, Ghent University—IMEC, Sint-Pietersnieuwstraat 41, B-9000 Gent, Belgium
[6] Physics, School of Engineering and Physical Sciences, Heriot–Watt University, Edinburgh EH14 4AS, UK
[7] SUSS MicroOptics SA, Jaquet-Droz 7, CP 42, CH-2007 Neuchâtel, Switzerland
[8] Korea Institute of Geoscience and Mineral Resources, PO Box 111, Daedeok Science Town, Taejon 305-350, Korea
E-mail: hottevaere@tona.vub.ac.be

Abstract

We review the most important fabrication techniques for glass and plastic refractive microlenses and we quantitatively characterize in a systematic way the corresponding state-of-the-art microlenses, which we obtained from selected research groups. For all our measurements we rely on three optical instruments: a non-contact optical profiler, a transmission Mach–Zehnder interferometer and a Twyman–Green interferometer. To conclude, we survey and discuss the different fabrication techniques by comparing the geometrical and optical characteristics of the microlenses, the range of materials in which the lenses can be produced, their potential for low-cost fabrication through mass-replication techniques and their suitability for monolithic integration with other micro-optical components.

Keywords: microlenses, interferometry, optical characterization, refractive optics, fabrication technologies

(Some figures in this article are in colour only in the electronic version)

1. Introduction

1.1. Microlens fabrication techniques: the timeline

In today's world of information processing the enabling role of optics and opto-electronics is becoming increasingly important as the performance of communication, processing, sensing and display systems is expected to be continuously enhanced. Making these photonic systems faster and smaller requires at the same time the introduction of massive parallelism and of micro-miniaturization. As a result high-quality, high-precision and low-cost microlens arrays are becoming indispensable

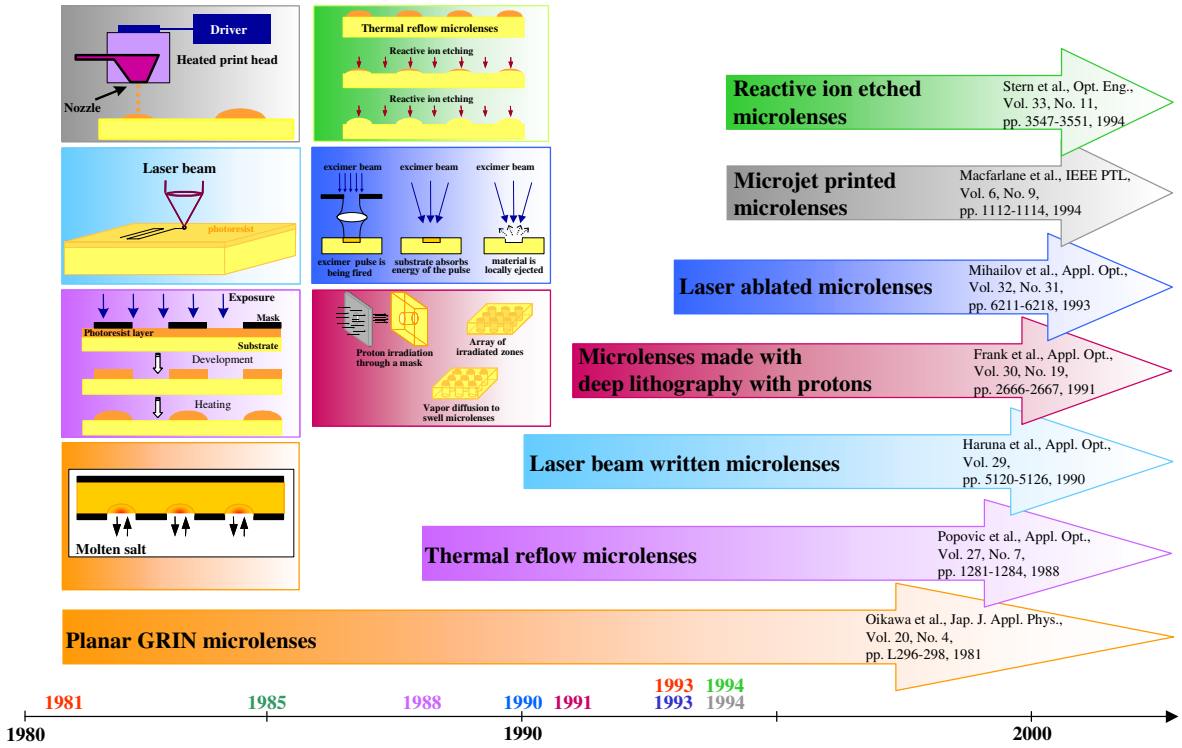

Figure 1. The microlens fabrication techniques and their development timeline which we will discuss in this paper.

components [1]. Over the last 15 years several research groups and industrial research laboratories have therefore been focusing their attention on the development of fabrication techniques for refractive microlenses and microlens arrays.

Microlens arrays made of glass have been studied for a relatively long time compared to those made in other materials. Various fabrication techniques have been proposed for this purpose [2]; among these are photothermal expansion [3], ion exchange [4], CO_2 laser irradiation [5] and reactive ion etching [6]. More recently fabrication techniques of micro-optical components in new lightweight optical materials have become the research topic of interest. Optical grade polymers in particular have attracted special attention because of the controllability of their mechanical and thermal properties and the fact that they can simplify the manufacturing process, leading to less expensive and superior components [7]. Several researchers have reported on fabrication methods for microlenses and lens arrays with these materials. They include techniques like photoresist reflow [8], laser beam shaping [9], deep lithography with protons [10], LIGA processing (German acronym for Lithographie, Galvanik und Abformung) [11], photopolymerization [12], microjet printing [13], laser ablation [14] and direct laser [15] or e-beam writing [16]. Some methods are relatively inexpensive and are based on existing technologies while others require dedicated processing tools and/or new materials with special properties. Most of these microlens fabrication methods yield microlens arrays that satisfy many of the optical quality requirements. They differ however in that some fabrication methods are more suitable either for rapid prototyping, for mass fabrication or for monolithic integration than others. In figure 1 we give an overview of the microlens fabrication techniques that we will discuss in this paper, by displaying each technology with its accompanying fabrication principle on a timeline.

1.2. Choice of lens materials and fabrication technologies

Microlenses and microlens arrays can be used for beam shaping purposes like collimation and focusing (e.g. in combination with laser-diode arrays, detector arrays or fibres), for illumination (e.g. in display systems and projection systems) and for imaging purposes (e.g. in photocopiers).

As a general rule we can say that the application will determine both the lens material and the fabrication technique to be used. The very first step in every microlens design and fabrication process therefore is the choice of the lens material: glass, plastic or semiconductor material [17]. Depending on the application it will be the combination of mechanical, optical, thermal or chemical requirements that will determine the material of choice. In certain cases the possibility to add mechanical features around the lens or lens array so that it can easily be integrated into a complete system, or the potential to be fabricated at lower cost or at a lower weight (for a given volume plastic can weigh two to five times less than glass [18]), will be of major importance. In that case plastics rather than glass materials will be the choice of preference. In most cases these advantages will outweigh some of the disadvantages of optical plastics, namely low mechanical strength, lower chemical and moisture resistance, larger thermal expansion coefficient α, larger dispersion (smaller Abbe number) [19] etc. The two most commonly used plastics are polycarbonate (PC) and poly(methyl methacrylate) (PMMA). As polymers and plastics nowadays become more and more used in a variety of optical components or in combination with power dissipating semiconductor structures,

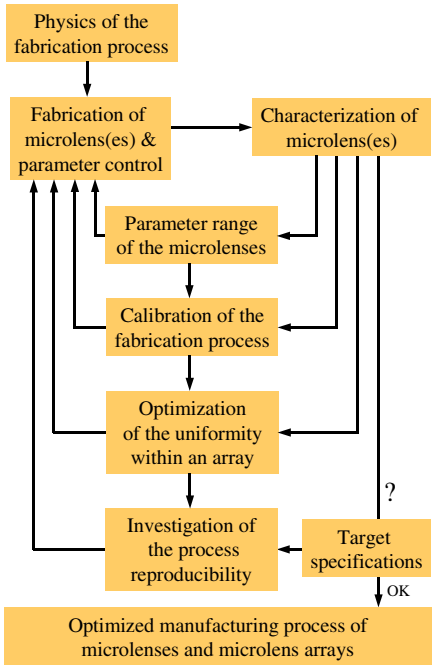

Figure 2. Flow chart of a microlens fabrication process.

the material specification requirements become increasingly demanding (e.g. higher glass transition temperatures T_g, lower thermal expansion coefficients α, higher optical transmissions OT, higher purity and lower moisture uptake to ensure constant optical properties,...). These demands challenge the polymer chemist to develop improved optical plastics like cyclic olefin copolymers (COCs) [17]. An overview of the characteristics of the most popular present-day optical plastics and their glass and semiconductor competitors is given in table 1. From these data it is clear that the family of COC plastics has a higher glass transition temperature and a higher optical transmission than the more classical plastics like PMMA, polystyrene (PS) and PC. Plastics also show thermal expansion coefficients that are an order of magnitude higher than those of glass, Si and GaAs. Still the general trend is that with the development of every new optical polymer, this family of optical materials is rapidly gaining importance over their glass contenders thanks to their superior characteristics and their potential as materials for low-cost mass-fabrication through hot embossing, injection moulding or vacuum casting [6].

It is clear that besides the selection of the material the choice of the fabrication technology is also closely linked either to the type of micro-optical component or to its specific application. Cylindrical microlenses for example obviously demand a different fabrication technique than spherical microlens arrays. Furthermore, some fabrication techniques like droplet-on-demand microjet printing lend themselves better to the heterogeneous integration of microlenses with opto-electronic assemblies, making it possible to be fully compatible with semiconductor processing lines. Finally, some fabrication technologies are unique in that they allow the monolithic integration of various micro-optical components, facilitating fabrication, replication, alignment and practical assembly.

1.3. Outline of this paper

In this paper we give a comprehensive overview of the most important fabrication methods for producing refractive microlenses. First we briefly introduce each technique and we compare the optical quality of different refractive microlenses. Although we will not be able to fully compare the performances of all the microlens fabrication methods we will assess the trends in performance for each technology. The order in which we discuss them is in accordance with their historical development, except for reactive ion etching of thermal reflow lenses. In the latter case we find it more relevant to include it in the section on thermal reflow lenses. Since our optical characterization instruments are not yet developed for semiconductor materials we have limited our study to glass and plastic microlenses.

Figure 2 shows the generic flow chart of a microlens fabrication process. It displays the logical sequence of the different steps to be taken from the underlying physics of the lens fabrication process to an optimized lens array manufacturing process. Before we discuss this flow chart it is important to distinguish between two approaches to microlens array fabrication: a first approach where discrete lenses are individually written using a sequential exposure process and a second approach where all the lenses of an array are written simultaneously.

In general, each microlens fabrication technique starts with the investigation of the underlying physical phenomena on which the technology is based. Once all the physical concepts are understood and materialized in a practical set-up, the fabrication of the prototype microlenses can start. For these very first microlenses an optical characterization is needed before further investigation can be undertaken. We noticed however that already at this early stage of the fabrication process some research groups do not go for a full optical characterization of their micro-optical components. Usually they stop the lens development at this level because of a lack of dedicated instrumentation. We will not include this type of work in our microlens survey as it does not build upon a solid scientific base.

Repeating the microlens fabrication for a large range of different process parameters allows us to investigate the multidimensional space of microlens characteristics that can be achieved with that specific technique. A careful mastering of the technology and a precise control of the experimental parameters then allows a calibration of the set-up which is needed to study the repeatability of the fabrication process. Before reproducibility can be examined, the process has to be enhanced to optimize the uniformity of the discrete lenses within one array. In a next step the process is repeated for a well determined set of calibration parameters. When the resulting microlens characteristics match the predefined specifications, the reproducibility of the fabrication process for that parameter range is demonstrated. However, if the specifications are not reached, the fabrication approach and the set-up should be revisited. Some of the microlenses, for example the microjet printed lenses, which we will characterize further in this work, were not yet fully calibrated at the time we started our investigations. Therefore, our measurements on these components will not only contribute to a comparative microlens survey, but the results will also

Table 1. Overview of common optical plastics [7, 18, 20–22].

		n_D (@589 nm)	T_g (°C)	ρ (g cm^{-3})	AH_2O (%)	α (10^{-5} °C)	OT (%)[a]	Spectral passing band (nm)[b]
Glass	BK7	1.517	559	2.51	[c]	0.71	99.9	350–1750
Semiconductors	GaAs[d]	3.3	1237	5.32	—	0.54	—	1000–14 000
	Si	3.5	1412	2.33	—	0.26	—	1500–5500
Plastics	Photoresist	1.63	90	1–1.1	0.5	6.4	—	500-1600
	UV epoxy	1.509	100–180	1.16	0.5–0.7	2.2	80–90	400–1600
	Poly(methyl methacrylate) PMMA	1.491	105	1.17	0.3	6.74	92	390–1600
	Polystyrene PS	1.59	110	1.06	0.2	6.0–8.0	87–92	400–1600
	Polycarbonate PC	1.586	130	1.2	0.15	6.6–7.0	85–91	360–1600
	Polyurethane	1.515	85	1.1	—	13	93	400–1640
	Cyclic olefin copolymer (e.g. Topas 5013)	1.533	140	1.02	<0.01	6.0–7.0	93	300–1600
	Cyclic olefin polymer (e.g. Zeonex E48R)	1.53	139	1.01	<0.01	6.0–7.0	92	300–1600

[a] Optical external transmission in the visible spectrum through a 3 mm thick plate.
[b] Spectral passing band for an optical transmission OT $> 90\%$.
[c] Good humidity resistance.
[d] All properties mentioned for GaAs are @10.6 μm.

further their individual calibration processes. Other microlens techniques like thermal reflow, RIE and laser beam writing had already fully completed the processing cycles as displayed in the flow chart when we undertook this comparison study. For these microlenses we will test whether the targeted specifications can be achieved.

2. Discussion of various microlens fabrication techniques and of the microlenses under test

Before discussing each microlens fabrication method we first list in table 1 the different technologies used by the research groups from whom we obtained representative samples. Then we have to quantitatively characterize the microlenses fabricated with these different technologies (see Table 2). In microlens testing it is essential to measure in a first step the shape or the surface profile of the microlenses or where gradient-index lenses are concerned their refractive index distribution. In addition the paraxial parameters, such as the focal length, and the more complex properties like the wave aberrations and surface quality have to be characterized. For arrays of microlenses the uniformity of the lenses and their mutual positioning accuracy may also be very important.

In [23] we discuss the different measurement instruments necessary to characterize all the geometrical and optical parameters. First we use a commercial optical non-contact profiler which we apply to determine the diameter and the sag of the surface profile microlenses. In addition it allows us to quantify the surface roughness on the top of the microlenses. With a transmission Mach–Zehnder interferometer we will measure the wave aberrations and the focal length of the microlenses, while we will use a Twyman–Green interferometer for the measurement of the surface deviations of a microlens from an ideal spherical shape and for the measurement of the radius of curvature of the surface. The two latter instruments were developed at the Erlangen–Nürnberg University. According to the lens quality criteria [1] we then decide whether the microlenses are showing a diffraction-limited optical performance. In a final section we assess each fabrication technique on the basis of the measured geometrical and optical characteristics, on the range of materials in which they can be produced, on the feasibility of replicating the microlenses and on the possibility of monolithic integration with other micro-optical components or structures. Whenever it is possible to study and compare the different fabrication technologies we characterize the microlenses for their full lens diameter as we wish. We are aware of course that for certain applications a smaller lens aperture is sufficient. In this latter case the aberrations will be smaller than the ones we will measure and discuss here.

2.1. Gradient-index microlenses

Gradient-index (GRIN) microlenses are a very special type of refractive optical elements and very different from surface profile microlenses. Indeed, rather than being refracted because of the surface profile, light in GRIN lenses is deflected by a refractive index gradient within the substrate. Two particularly interesting lenses are the GRIN rod lens (see figure 3(a)), which is widely used in optical imaging and fibre coupling systems, and the planar GRIN microlens with a 3D index distribution (see figure 3(b)). There are several basic techniques for obtaining microlenses with the required refractive index distribution in a glass or plastic substrate: selective exchange of ions in a suitable glass substrate [4], diffusion polymerization in plastics [24], chemical vapour deposition, neutron irradiation, ion stuffing and crystal growth [25].

In this section we will only discuss that particular ion exchange process which lies at the basis of most of the commercially available GRIN lenses. For other ion exchange

Table 2. Overview of various microlens fabrication techniques, the lenses of which are characterized and discussed in this paper.

Fabrication technique	Material	Samples provided by
Ion exchange	Glass	Nippon Sheet Glass (NSG), Micro-optics Group, Japan http://www.nsg.co.jp/english/moc/
Thermal reflow	Photoresist	Institute of Microtechnology of the University of Neuchâtel, Department of Applied Optics, Switzerland http://www-optics.unine.ch/
Reactive ion etching of thermal reflow lenses	Fused silica	Heriot–Watt University, Department of Physics, UK http://www.phy.hw.ac.uk/
Reactive ion etching of thermal reflow lenses	Fused silica	McGill University, Department of Electrical and Computer Engineering, Canada but fabricated by MEMS Optical Inc. http://www.memsoptical.com/
Reactive ion etching of thermal reflow lenses	Fused silica	Suss MicroOptics, Switzerland http://www.suss-microoptics.com/
Reactive ion etching of thermal reflow lenses	Fused silica	RICOH Company, Research and Development Group, Japan http://www.ricoh.com/
Direct laser writing	Polymer (confidential)	Heptagon, Finland–Switzerland http://www.heptagon.fi/
Deep lithography with protons	PMMA	Institute of Geology, Mining and Materials, Korea http://www.ionbeam.kigam.re.kr/
Deep lithography with protons	PMMA	Vrije Universiteit Brussel, Department of Applied Physics and Photonics, Belgium http://www.tona.vub.ac.be/
Laser ablation	PC	Universiteit Gent, Department of Information Technology, Belgium. http://www.intec.rug.ac.be/groupsites/opto/
Microjet printing	Epoxy polymer	MicroFab Technologies Inc., Texas, USA http://www.microfab.com/

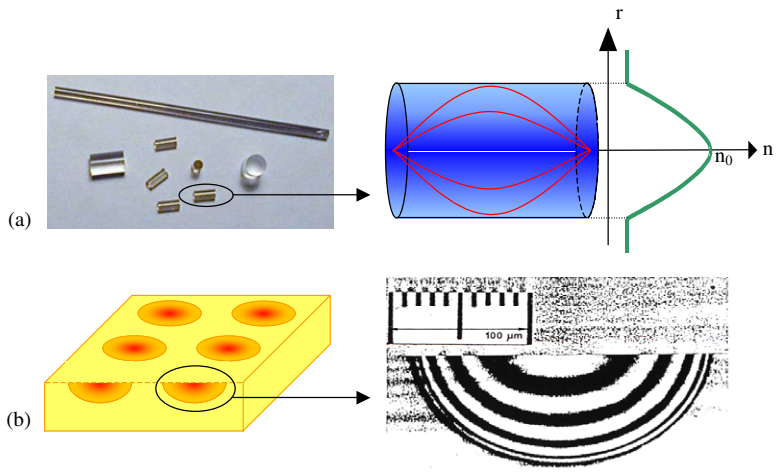

Figure 3. (a) Several GRIN rod lenses [28], point-to-point imaging through a GRIN rod lens with pitch $P = 0.5$ and the radial refractive index distribution in a GRIN rod lens; (b) array of planar GRIN microlenses and the index distribution of a planar microlens [29].

techniques we refer to the literature. During an ion exchange process the substrate, usually a glass with well specified properties, is shielded with a mask to protect it against undesired ion exchange, except at small circular apertures that define the footprints of the planar microlenses.

Then the substrate is immersed in a bath of an appropriately chosen molten salt, the metal ions of which diffuse into the glass matrix. There they replace some of the silicon, sodium or potassium atoms, depending on the type of glass used. Because ion exchange is an isotropic process, a radially symmetrical ion concentration profile is generated, which causes a refractive index distribution of the corresponding shape. The rate of ion exchange at a given location and the resulting change in refractive index depend on the ion-dopant concentration, leading after a particular time to the desired gradation of refractive index from the surface to the bulk of the glass substrate. Some modifications to this ion exchange process have been applied to optimize the resulting index profiles. An example hereof is the mask structured ion exchange (MSI), where an appropriate mask structure (e.g. a lithographically structured mask with 1.5 μm diameter apertures) is used to enhance the control over the three-dimensional index distribution [26]. Furthermore, field-assisted ion exchange, also called electromigration [27], can

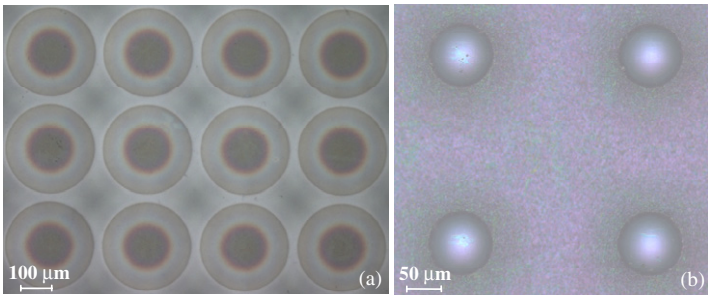

Figure 4. (a) Part of the array of 240 μm diameter planar microlenses; (b) part of the non-planar microlens array with 85 μm diameter lenses.

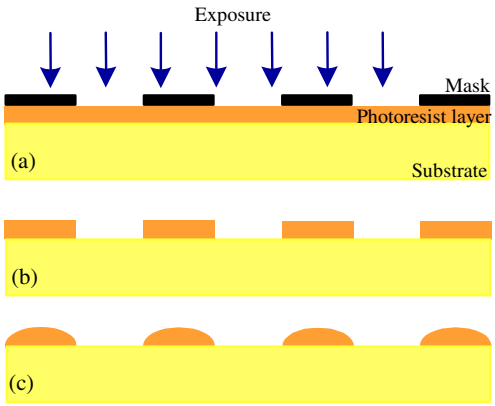

Figure 5. The different fabrication process steps for refractive reflow photoresist microlenses: (a) patterning of the photoresist layer; (b) development of the exposed regions; (c) melting of the cylindrical islands.

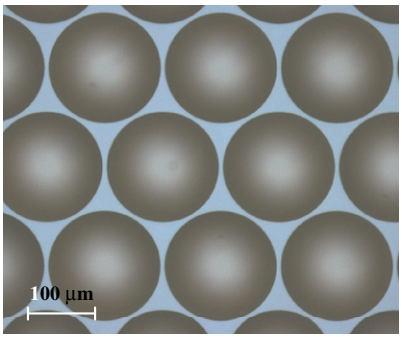

Figure 6. Part of the microlens array with 145 μm diameter photoresist microlenses.

increase the ion mobility through the use of an electric field across the interface between the substrate and the salt melt. Due to this electric field, the movement of the ions from the melt into the substrate is accelerated and the penetration depth of the ions is significantly increased.

Table 3 summarizes the most important published geometrical and optical characteristics of both the rod and the planar GRIN lenses. The GRIN rod lenses, because of their good imaging properties, have many applications in photocopiers, facsimile systems and bar-code readers. They are also often used in optical communication systems in combination with optical fibres for light coupling purposes. Planar GRIN microlenses where the light is also deflected by a refractive index gradient and not by a surface shape have the advantage that they can easily be stacked and cemented onto other passive components or interfaced with opto-electronic devices. On the other hand, gradient index optical components have the important drawback that they cannot be replicated.

The gradient index planar microlenses that we investigated in our comparative study are microlenses fabricated with ion exchange technology. The microlens array samples are provided by Nippon Sheet Glass (NSG), Japan. The first sample contains 240 μm diameter lenses with a focal length of 650 μm (see figure 4(a)). The second array consists of 85 μm diameter microlenses with a focal length of 115 μm (see figure 4(b)). The latter microlenses are also fabricated with ion exchange but an additional curvature is created on the surface by swelling each lenslet to increase its numerical aperture [30]. This swelling is mainly caused by the use of a different type of ions, which occupy a larger volume.

2.2. Thermal reflow or resist melting method

2.2.1. Fabrication of thermal reflow microlenses. The thermal reflow process has been for many years the only commercial available approach for the fabrication of large arrays of hemispherical microlenses and is therefore most probably the best-known method. In this particular case plastic refractive microlenses are fabricated by melting cylindrical islands of a photoresist or a similar polymer [8]. To this end a glass substrate is first coated with a layer of this photoresist. The thick layer is then patterned lithographically [32] and developed to form a series of cylindrical islands, which are then heated above the glass transition temperature of the photoresist. Due to surface tension the shape of the photoresist cylinders changes to minimize the surface energy. As a result hemispherical microlenses are formed (see figure 5). This technology has also been extended to yield arrays of cylindrical lenses and lenses with a square footprint [33].

Photoresist microlenses, although covering a wide parameter space, are limited by certain physical phenomena. As a consequence, not all ratios between the lens diameter and the photoresist thickness, and thus the sag of the microlenses, can be used to generate a spherically shaped photoresist cap. A first example is when the photoresist thickness is too low. This leads to significant deviations from a spherical shape at the vertex of the microlens and an important degradation of its optical performance. Hence microlenses with a low

Table 3. Most important properties of GRIN microlenses made by different ion exchange methods.

GRIN microlenses	D (μm)	NA	f (μm)	f#	SA (λ)	Strehl ratio	Ref.
GRIN rod lens	>1000	0.1–0.6		0.7–5			[29]
Planar GRIN microlens							
Na^+/Tl^+ field-assisted ion exchange	10–1000	0.02–0.25	20–4000		3.429	0.05	[30]
Na^+/Tl^+ ion exchange with surface swelling	10–400	<0.57	55–500				[30]
Na^+/Ag^+ ion exchange	20–3000	0.036-0.06	100–100 000				[26, 31]
Na^+/Ag^+ field-assisted ion exchange	20–800	<0.2	100–2000				[26]

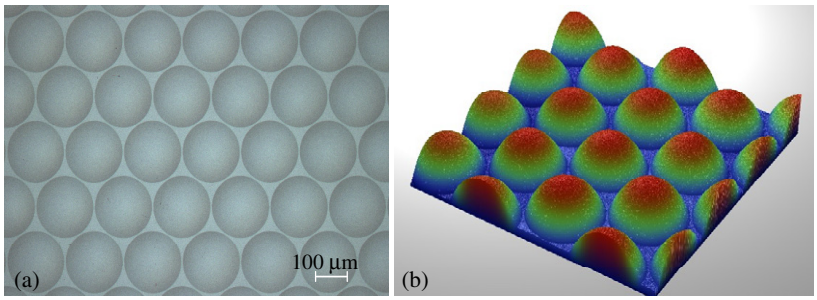

Figure 7. (a) Part of the array with 200 μm diameter RIE microlenses and (b) a 3D representation of this microlens array.

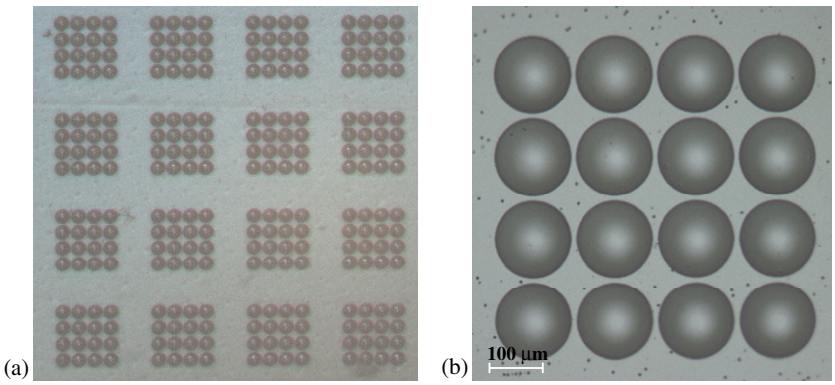

Figure 8. (a) Part of the sample with 16 4 × 4 arrays of 123 μm diameter microlenses; (b) detail of a 4 × 4 microlens array.

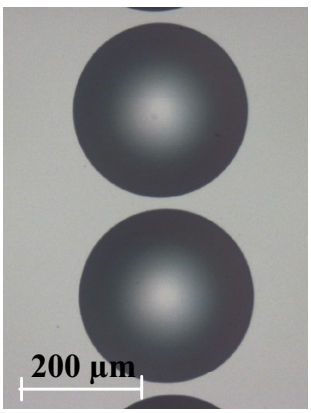

Figure 9. Two microlenses out of the 1 × 48 array of 238 μm diameter microlenses

numerical aperture (NA $<$ 0.15) cannot be fabricated. A solution here is to add a layer on top of the substrate to influence the surface tension between the substrate and the photoresist, thus decreasing the critical angle [34]. With these techniques one is able to extend the range of numerical apertures of these lenses from 0.15 to values down to 0.1. Preshaping is another way to increase the parameter range of the microlenses but now to achieve very fast microlenses [9]. The difficulty of fabricating a thick resist coating is a second illustration of how the minimum required ratio between the photoresist thickness t and the lens diameter $D(t/D > 1/23)$ can restrict the microlens parameter range. In most cases it will limit the maximum achievable lens diameter to 1000 μm [29]. The minimum lens diameter on the other hand is limited by standard photolithography to 2 μm [35]. On top of this, the uniformity of the resist thickness has to be very high to achieve uniform microlenses after the melting process.

Two samples containing photoresist microlenses with a diameter of 145 μm and a sag of 20 μm were provided by the Institute of Microtechnology in Neuchâtel (see figure 6).

2.2.2. Transfer of microlenses in other materials via reactive ion etching (RIE). Some photoresists are not ideally suited as microlens material in particular applications. This is mainly

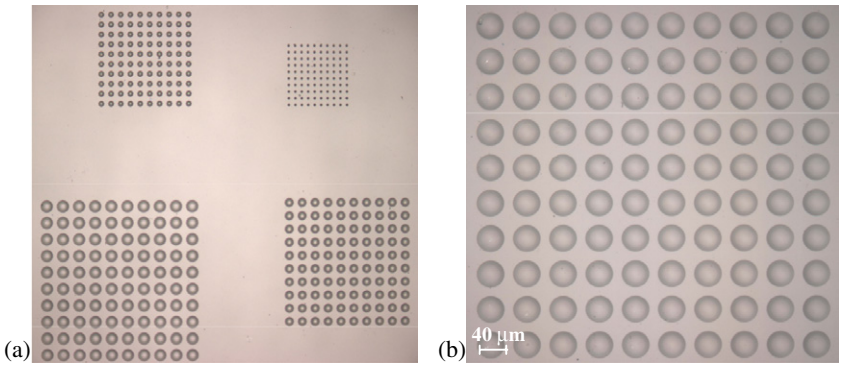

Figure 10. (a) Picture of four 10 × 10 microlens arrays with diameters of respectively 10, 20, 30 and 40 μm; (b) zoom-in of the array with 40 μm diameter lenses.

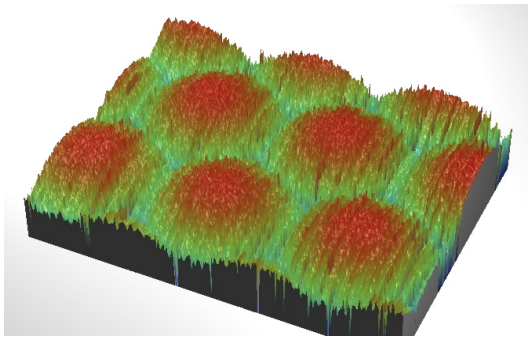

Figure 11. 3D profile of a part of the hexagonally packed microlens array clearly showing the parallel lines along which the lenses are written.

due to their limited thermal and mechanical stability and their relatively large absorption. Therefore efforts have been made to transfer the surface profile of the microlenses into more stable substrate materials like fused silica or semiconductors. One approach is the use of reactive ion etching (RIE) to simultaneously remove atoms from the photoresist surface and the substrate material until the microlens shape is completely transferred to the substrate [36]. For applications in the visible and the UV wavelength regions, the resist lenses are usually transferred in fused silica whereas silicon or GaAs are applied when microlenses are to be used in the IR wavelength region [34]. In addition to changing the material system this dry etching transfer step also allows us to modify the geometry of the refractive microlenses, such as an increase or a reduction of the vertical dimension of the microlens structure, through a control of the selectivity of the etching process [35].

In this paper we will measure and compare the characteristics obtained on RIE microlenses from four different research groups. The first sample with photoresist microlenses transferred in fused silica via RIE (see figure 7) was provided by the Department of Physics of the Heriot–Watt University. These microlenses feature a diameter of 200 μm and a focal length of 1.9 mm.

The Department of Electrical and Computer Engineering of the McGill University provided us with a second array of RIE microlenses, originally fabricated by MEMS Optical Inc. (see figure 8). The sample contains 32 arrays of 4 × 4 microlenses each with a diameter of 123 μm, a focal length of 246 μm and a pitch of 125 μm.

Suss MicroOptics SA provided another array of photoresist microlenses transferred in fused silica via RIE. The array contains 48 microlenses with a diameter of 238 μm and focal length of 215 μm. Two microlenses from this array are displayed in figure 9.

One sample containing four arrays of photoresist microlenses transferred in fused silica via RIE were provided by the RICOH Company. Each array consists of 10 × 10 microlenses with diameters of respectively 10, 20, 30 and 40 μm (see figure 10) and a focal length of 120 μm. Only the latter array will be characterized because for diameters lower than 30 μm diffraction effects and imaging problems will prevent reliable interferometric measurements. We should remark here that making microlenses over a wide range of diameters on the same sample with this technology will not result in high-quality lenses for all diameters since there is an optimum photoresist thickness range for each microlens diameter.

2.3. Direct written microlenses

Direct writing techniques make use of precision-steered beams to locally expose photoresist films. The controlled exposure of such a photoresist film enables a wide variety of micro-optical components to be produced. The underlying idea here is that the photoresist must be exposed and processed such that the local thickness of the developed resist film is a continuous and preferably linear function of the energy deposited by the beam [15]. These direct writing techniques are of particular interest for the fabrication of planar continuous relief and hybrid microlenses, especially since the latter type, made up of a combination of refractive and diffractive surface structures, is difficult to fabricate with earlier discussed techniques like thermal reflow. Another asset of this approach is that a suitable choice of the photoresist material allows the use of well established, commercially available, semiconductor lithography equipment. Different types of direct writing techniques exist: direct laser writing [15], electron beam [16] and focused ion beam writing [37], and laser ablation [14]. For the sake of completeness, the fabrication by half-tone mask imaging [15, 38]—although not strictly a direct writing technology—should also be mentioned.

To illustrate the direct writing technique, we focus on the fabrication of refractive microlenses by laser beam writing. The first step in the fabrication process of such a microlens

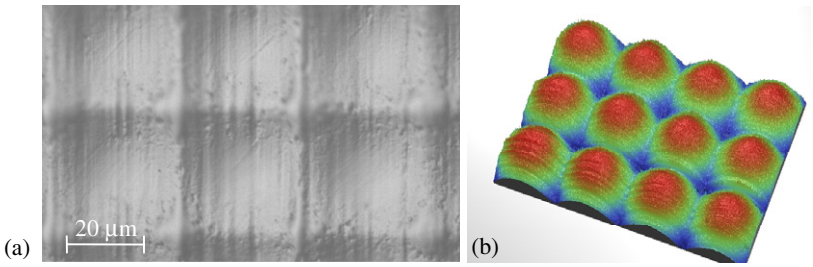

Figure 12. (a) Part of the squared packed microlens array and (b) its 3D representation measured with a non-contact optical profiler.

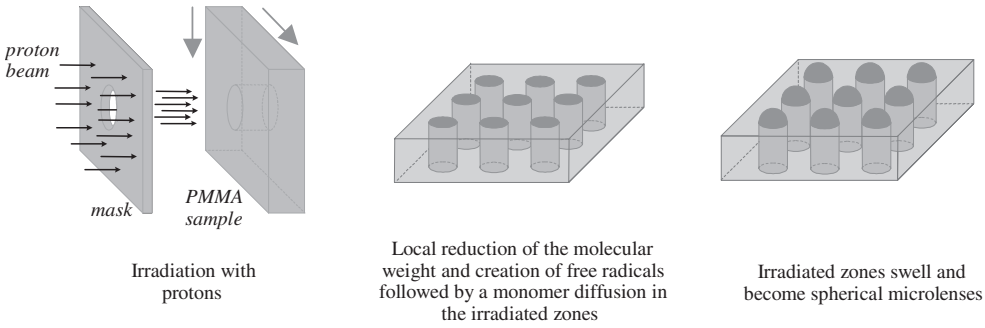

Figure 13. Basic fabrication process for arrays of spherical microlenses with deep lithography with protons: irradiating the PMMA layer through a mask and applying a vapour on one surface of the irradiated sample are the basic processing steps for the fabrication of 2D arrays of stable and uniform spherical microlenses.

is the generation of the surface relief data corresponding to the desired microlens specifications. The data usually obtained with custom or commercial optical design programs are then converted to laser beam intensity values. To do so one uses calibration curves that relate the deposited optical energy on the resist to the corresponding relief height of the resist film after development. The exposure is realized by moving the resist-coated substrate under a focused HeCd laser beam ($\lambda = 442$ nm) using accurate translation stages while synchronously modulating the laser beam intensity to write a continuous, greyscale pattern in the photoresist. A controlled development of the exposed resist film finally results in the desired microlens profile. The major advantage of the direct writing technique lies in the potential to fabricate microlenses with characteristics that can be tailored for every lens individually. Once such a microlens array is fabricated low-cost copies can be mass-produced using replication techniques.

Two arrays of refractive microlenses which we will investigate in this section were fabricated with a HeCd laser beam by Heptagon[9]. The microlenses are made with a specialty polymer on a boro-float glass substrate. The polymer (refractive index $n = 1.557$ @ 633 nm) is intellectual property of Heptagon and further specifications have not been disclosed to us. The first array consists of microlenses with a hexagonal footprint and are specified to feature a size of 216.8 μm, a focal length of 3500 μm and a focal number of $f\# = 16$ [39].

A second examined array of lenses consists of microlenses with a square footprint, a size of 30 μm and a focal length of 200 μm. After a geometrical characterization we find that the individual elements have a size of 30 μm, a relief height of 1.59 μm and an RMS surface roughness of 22.29 nm (see figure 12).

[9] The continuous-relief microlenses with a hexagonal and a square footprint were purchased from Heptagon, Switzerland–Finland.

2.4. Microlenses fabricated with deep lithography with protons (DLP)

The concept of the DLP process is based on the fact that protons, which penetrate a sample made of linear high-molecular-weight PMMA, will split the long polymer chains [40]. As a consequence the molecular weight of the material located in the irradiated zones will be reduced and free radicals will be created, resulting in material properties that are very different from those of the bulk. Next the irradiated domains can be swollen using a monomer vapour. Indeed, because of the lower molecular weight of the PMMA material in the irradiated zones of the sample, the diffusion velocity for small molecules will be much larger than in the non-irradiated bulk material. This selective diffusion process will cause a considerable expansion of the irradiated volume, which for circular footprints will result in hemi-spherical surfaces. After diffusion into the PMMA sample the monomers will bond to the irradiation-induced free radicals and as a consequence will be fixed in the sample. This process permits the fabrication of stable hemispherical microlenses with well defined sags.

The basic concept of DLP finds its roots in the Department of Physics of the Erlangen–Nürnberg University where its proof of principle was demonstrated for the first time in 1990 [41]. Our laboratory at the VUB adopted this DLP technique in 1996, thoroughly upgraded its practical implementation, improved its performances, extended its range of practical applications and turned it into a generic high-quality MOMS technology. Some years ago researchers of the Institute of Geology, Mining and Materials in Korea also

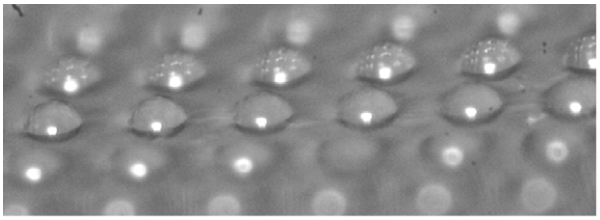

Figure 14. Part of an array of 200 μm diameter spherical microlenses (diffusion temperature $T = 70\,^{\circ}$C, diffusion time $t = 40$ min).

started with the fabrication of microlenses based on the DLP method [42].

In this paragraph we highlight the main differences in the irradiation process between the two approaches. A first difference is that in the Korean set-up the protons are generated by a tandem accelerator while we make use of a cyclotron to create the protons. The main difference between the two proton sources is the higher spatial beam stability of the tandem accelerator for the proton beam. Indeed the protons in a tandem accelerator are accelerated in a linear set-up while in a cyclotron the protons are accelerated using D-shaped structures. We have partially tried to compensate the higher instability of the proton beam in our set-up by a high accuracy measurement of the proton fluence during irradiation. For the microlenses discussed in this section the proton energy used in Korea was 3 MeV whereas at the VUB we used 8.3 MeV, since this is the lowest energy for the stable operation of the cyclotron to produce a proton beam. Because the swelling of microlenses is a surface effect low energy protons with a short penetration depth are sufficient. This means that the thickness of the mask to stop the protons can be much thinner. It is therefore easier to fabricate apertures in the proton masks with a higher geometrical accuracy. The Korean group therefore makes use of a 100 μm thick stainless steel mask with circular apertures of 125, 175 and 250 μm in diameter instead of the LIGA mask that we use which features a thickness of 300 μm and circular apertures ranging from 20 to 1000 μm. We expect that the difference in energy will make no difference if we focus on the fabrication of microlenses only. After the irradiation session the samples are annealed at 90 °C for 1 h to relax the internal stresses and to decrease the number of cracks on the substrate surface in preparation of the diffusion process. During the diffusion, the samples are exposed to a monomer vapour at a temperature between $T = 60$ and 90 °C, while the diffusion times can vary between $t = 30$ and 60 min. Finally, the samples are stabilized by a UV exposure for 20 min.

A first sample with DLP microlenses was fabricated at the VUB and contains 200 μm diameter lenses with different focal lengths ranging between 160 and 1400 μm. A part of the microlens array is shown in figure 14.

Different samples obtained from the Institute of Geology, Mining and Materials were characterized. The samples, each consisting of 15 microlenses with diameters of 125, 175 and 250 μm, were fabricated with different process parameters. As an example a DLP microlens with a diameter of 175 μm is shown in figure 15.

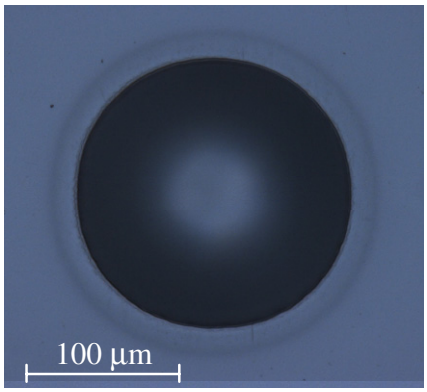

Figure 15. Detail of a 175 μm diameter microlens ($T = 75\,^{\circ}$C, $t = 40$ min).

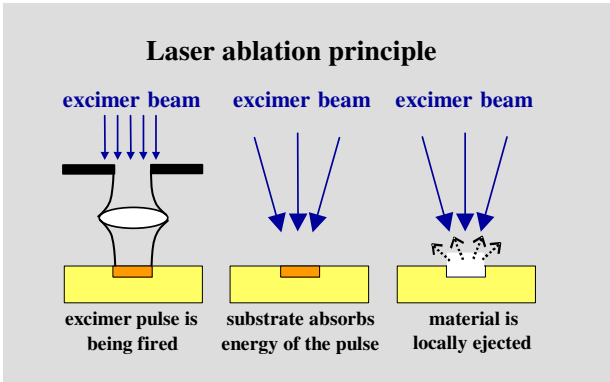

Figure 16. Principle of laser ablation.

2.5. Laser ablated microlenses

In the last decade, excimer laser ablation acquired the reputation of being a reliable technology for the fabrication of microstructures. This non-resist technique does not require clean-room facilities, can be applied on a broad range of materials and is potentially fast since it allows parallel microstructuring by means of mask patterns. This means that the technique is suited both for prototyping and for fabricating microparts in small numbers, or for applications where conventional tools like mechanical drilling lack the necessary accuracy. Additionally, this fabrication technique can be applied for non-contact precision tooling purposes in one of the last fabrication steps or in the post-processing of heterogeneously assembled opto-electronic or photonic components [43].

The principle of excimer laser ablation is based on precision removal of substrate material and works as follows. A focused excimer laser (both wavelengths of 248 and 193 nm can be used) illuminates a mask. The image of this mask is projected onto the substrate. If the irradiated material absorbs energy above a certain threshold it will be spontaneously vaporized (see figure 16). This process is called photoablation. Materials such as metals, optical glasses, plastics and ceramics have already been used to produce microstructures [44]. A typical ablation system has a configuration similar to that required for laser beam writing in photoresist (see section 2.3),

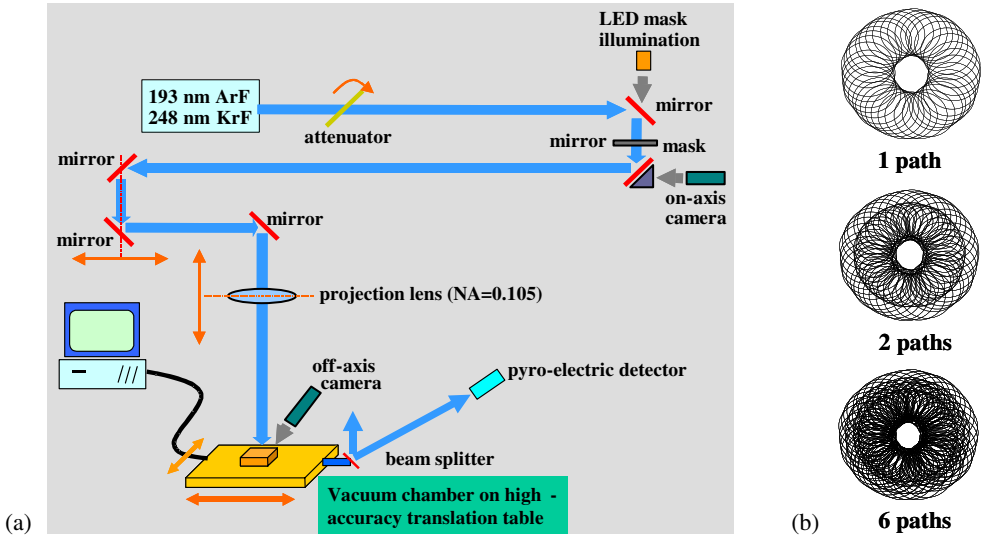

Figure 17. (a) Laser ablation set-up used in the Department of Information Technology at the Universiteit Gent [48]; (b) circular concentric movements to fabricate microlenses after writing a different number of paths.

except that the modulator is replaced by a programmable pulse generator for driving the UV excimer laser.

The fabrication of refractive microlens arrays using an excimer laser operating with an ArF gas mixture ($\lambda = 193$ nm) has been described by Mihailov *et al* [45]. Their approach consisted in using the ablation process to partially remove material of a doped Teflon layer spin coated on a fused silica or silicon substrate such that islands of this polymer are formed. Then they applied a thermal reflow process. The microlenses they obtained varied in diameter size from 50 to 385 μm with numerical apertures between 0.2 and 0.3 and focal lengths ranging between 100 and 650 μm. In a similar way but with less complicated process steps Beinhorn *et al* demonstrated the fabrication of microlens arrays, generated by UV laser irradiation of doped PMMA and followed by a subsequent matrix softening [46]. To fabricate refractive microlenses along the ablation principle we just described, one needs complex mask patterns [47]. A different technique to fabricate micro-optical structures in general and refractive microlenses in particular is the use of direct ablation with a single circular aperture as mask. Here the shape of the structure is determined by the movements of the translation stage on which the sample is placed and is not restricted to any particular circular symmetric shape. For the fabrication of microlenses the pulse energy and the pulse frequency of the laser remain constant during the ablation process. While the excimer laser is firing pulses, the translation stage makes circular concentric movements with different radii and speeds. By carefully choosing both the speed and the radius, one can obtain any desired surface shape with circular symmetry (see figure 17) [48]. Next a larger aperture is been used for cleaning and smoothing the laser machined surface [49]. This post-processing step spatially averages the optical power over the aperture, thus allowing us to accomplish debris removal.

The Department of Information Technology (INTEC) of the Universiteit Gent provided a sample with 200 μm diameter polystyrene microlenses with varying radii of curvature (101–700 μm). We have determined both the sag and the diameter of

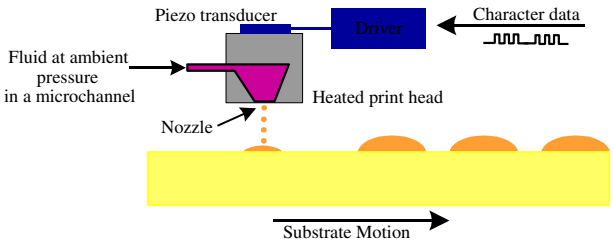

Figure 18. Schematic of the droplet-on-demand microjet system used to fabricate refractive microlenses.

the microlenses with a non-contact optical profiler on the basis of their 2D profiles. In this case the measuring instrumentation shows a lateral resolution of 0.63 μm. Because there is only one microlens for each radius of curvature, we cannot investigate the uniformity of the sag within an array of identical microlenses or the reproducibility of the laser ablation method. This means that the measurements we performed are currently used as part of the laser ablation calibration process.

2.6. Microjet printed microlenses

Microjet technology, originally developed for low-cost desktop printing, has recently been adapted for the fabrication of microlenses [13]. One can distinguish two types of microjet devices. A first one yields the physically interesting situation of generating a continuous stream of fluid which breaks apart into droplets during its travel from the aperture to the target substrate. A second type of device generates individual liquid droplets at a well controllable frequency. Both the precision and the flexibility of this second approach, better known as the droplet-on-demand (DOD) microjet technology, make it more apt to be used in lens manufacturing applications.

With the latter technique arrays of refractive microlenses with a circular substrate footprint have been fabricated by printing the precise number of droplets required for the lenslet

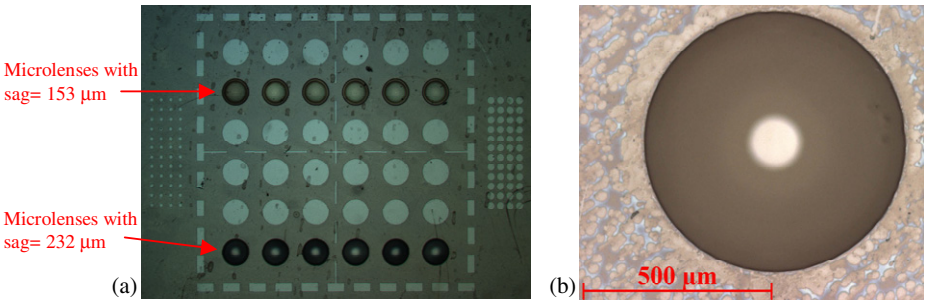

Figure 19. (a) Array in which only two rows of spherical microlenses with a diameter of 700 μm and varying sags are printed; (b) detail of such a 700 μm diameter microlens.

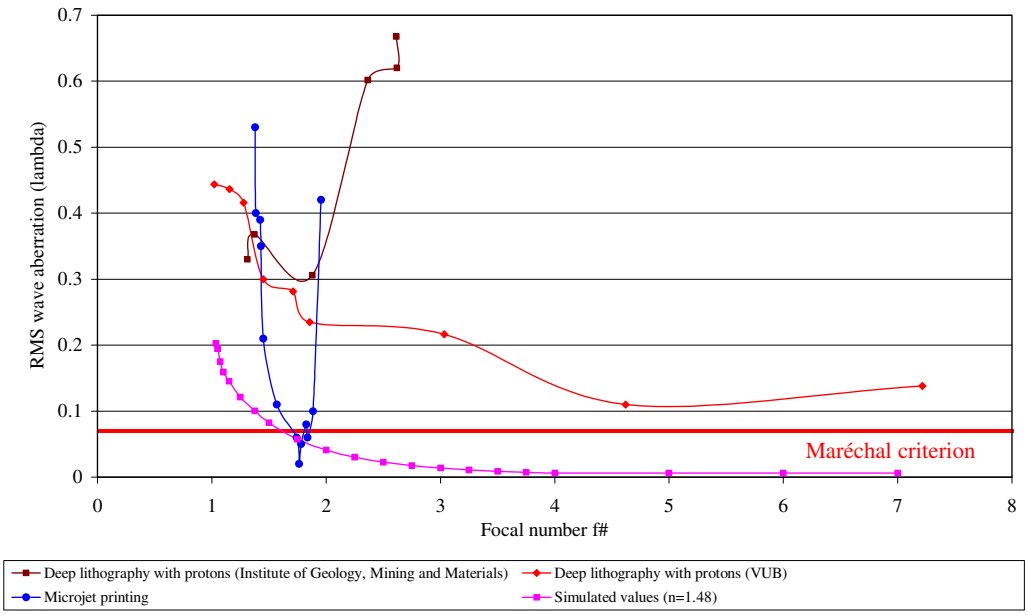

Figure 20. RMS wave aberrations (lambda) as a function of the focal number $f\#$ for all characterized microlenses ($\lambda = 632.8$ nm; the simulated values are obtained for a 200 μm diameter lens).

volume at predetermined locations on a target substrate. The microjet printing head is made of a piezoelectric ceramic featuring a microchannel (see figure 18). This microchannel connects a reservoir containing the polymer liquid to a nozzle that directs the liquid to be ejected towards the printing surface. Digital voltage signals drive the print-head by causing a contraction of the piezoelectric ceramic so that polymer droplets are ejected from the nozzle. The number of droplets applied per microlens controls the liquid volume dispensed for each microlens. These droplets hit the substrate and get together to form spherical caps, acting as plano-convex microlenses. The substrate is fixed to a translation stage to control the position of the deposited droplets and thus the location of the microlens. Temperature control of the reservoir and the substrate allows us to control the viscosity of the dispensed liquid and its cooling off on the substrate. Substrate surface treatment processes, such as the application of non-wetting layers, furthermore enable the control of the microlens spacing and the lens diameter. Since all these parameters directly influence the surface tension, they also yield control over the resulting lens shape.

The materials best suited for DOD microlens fabrication are UV curing optical epoxies because of their thermal and chemical durability as compared to other optical-grade plastics such as photoresists, acrylics and thermoplastics [50]. Microlenses ranging in diameter from 20 μm to 5 mm have been fabricated with this method [51]. Microlens speeds may be varied for a given diameter over a wide range ($f\# = 1.5$–10), even within the same array [52]. Refractive microlens configurations which have already been microjet printed range from plano-convex hemispherical, hemi-cylindrical, hemi-elliptical and square to the convex–convex configuration where two plano-convex lenslets are coaxially printed on opposite sides of a substrate. Recently, researchers from MicroFab Technologies have shown that they can even fabricate gradient-index lenses by sequentially depositing two optical epoxies with a different index of refraction at the same location [53]. Microjet printing is therefore a fully automated, data-driven process with which microlenses may be written directly onto optical substrates and components such as diode lasers, optical fibres and waveguides. This process can also be used in other optical application areas such as organic LED displays and optical fibre biochemical sensors [52].

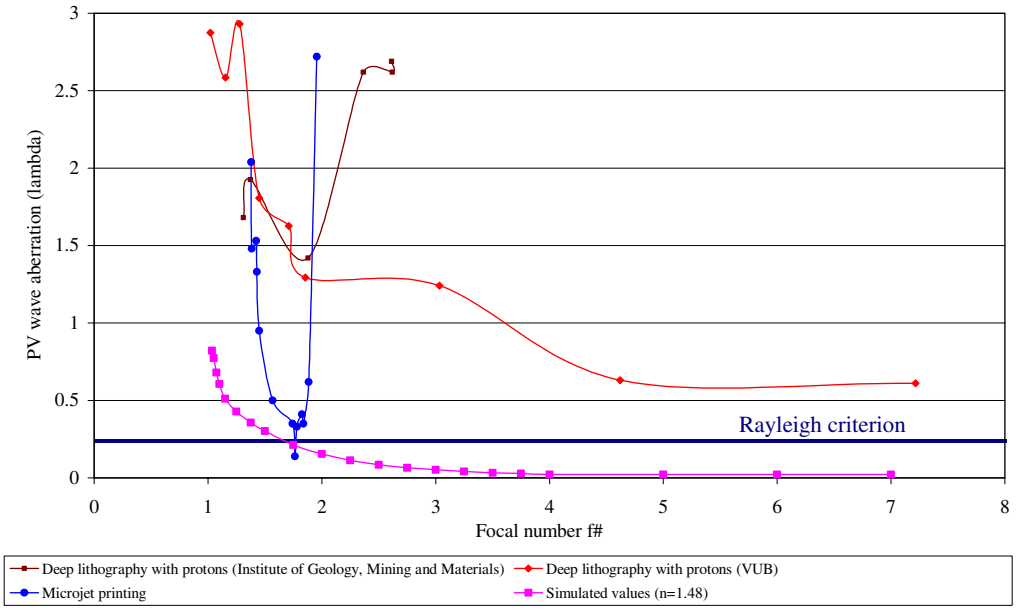

Figure 21. PV wave aberrations (lambda) as a function of the focal number $f\#$ for all characterized microlenses ($\lambda = 632.8$ nm; the simulated values are obtained for a 200 μm diameter lens).

A substrate with different arrays of 700 μm spherical microlenses with polyether thermoset optical plastic as lens material was provided by MicroFab Technologies Inc. (see figure 19). Since the lens diameter (700 μm) is determined by the surface treatment and the drop size (43.6 μm) is predetermined by the printing system, there is only one fabrication parameter left during the printing operation, namely the number of drops. On the sample under investigation the number of drops was modified from one microlens array to the other between 300 and 1400 drops while the microlenses within one array are all printed with the same number of drops. The goal of our geometrical and optical measurements here is to calibrate this microjet printing process. With that aim we measured a single microlens out of each of the microlens arrays that contained identical lenses, except for the arrays of greatest interest for MicroFab Technologies. In the latter case the measurements of the sag of the lenses provided a measure for their uniformity within an array.

3. Discussion and comparison of refractive microlenses manufactured with different fabrication techniques

In this section we compare the characteristics of the microlenses that were manufactured with those fabrication methods that we have been discussing up to now in this paper. We will proceed as follows. In a first step we assess and compare each microlens fabrication technique on the basis of the measured optical characteristics of the resulting microlenses. Then we review for the highest quality microlens of each technology the ratio of the surface roughness/sag, the RMS and PV wave aberrations, the modulation transfer function, the point spread function and the Strehl ratio, and the deviation from a perfect sphere. After a discussion of these microlens characteristics we compare the experimental microlens characteristics to the values achieved with ray-tracing software for perfect spherical microlenses with identical geometrical characteristics. Finally we complete our quantitative study by summarizing the fabrication parameter ranges for each of the microlens fabrication techniques based on values found in the literature.

Before discussing the microlens characteristics we first explain briefly the Rayleigh and Maréchal criterion, of which a more extensive explanation can be found in the literature [1]. The widely used Rayleigh criterion states that a system is diffraction limited as long as the maximum wavefront deviation $|\psi_{\max}(x)|$ is less than one-quarter of a wavelength. This criterion, which determines the amount of aberration that can be tolerated in an image-formation system, is of course only a rough guideline since the light distribution in the image does not only depend on the maximum deformation but also on the shape of the wavefront, and more particularly on the type of aberration. Moreover, the loss of light that can be tolerated depends on the particular use to which the optical component is put, and more stringent tolerances have to be imposed for certain applications. This Maréchal criterion uses the following root-mean-square wavefront aberration ψ_{RMS} to define the lens quality:

$$\psi_{\mathrm{RMS}} = \sqrt{\int |\psi(x)|^2 \, \mathrm{d}x - \left[\int |\psi(x)| \, \mathrm{d}x\right]^2} \leqslant \frac{\lambda}{14}.$$

This criterion is sensitive to statistical noise on the measured phase profile, while a criterion such as the Rayleigh criterion is little affected by it.

To start with we have plotted in figures 20 and 21 the measured RMS and PV aberrations as a function of the focal number for those microlens fabrication techniques for which we obtained samples containing lenses with different focal numbers. Additionally, we displayed the theoretical aberration behaviour as a function of the focal number for

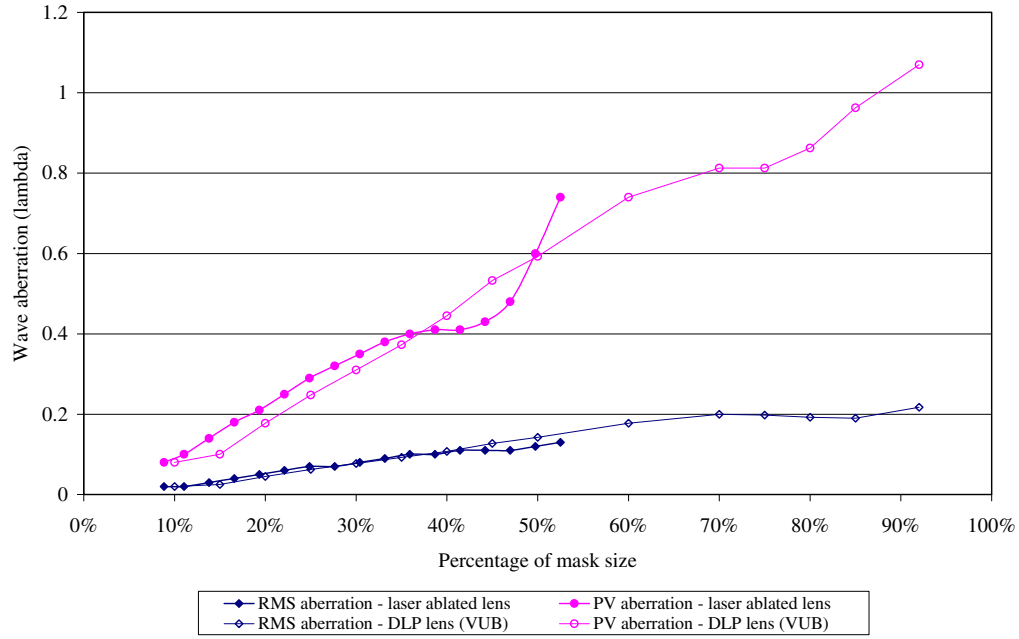

Figure 22. The influence of the mask size on the RMS and PV wave aberrations (lambda) for a laser ablated microlens and a DLP lens (VUB) with identical characteristics ($D = 200\ \mu$m; $f = 1283\ \mu$m) ($\lambda = 632.8$ nm).

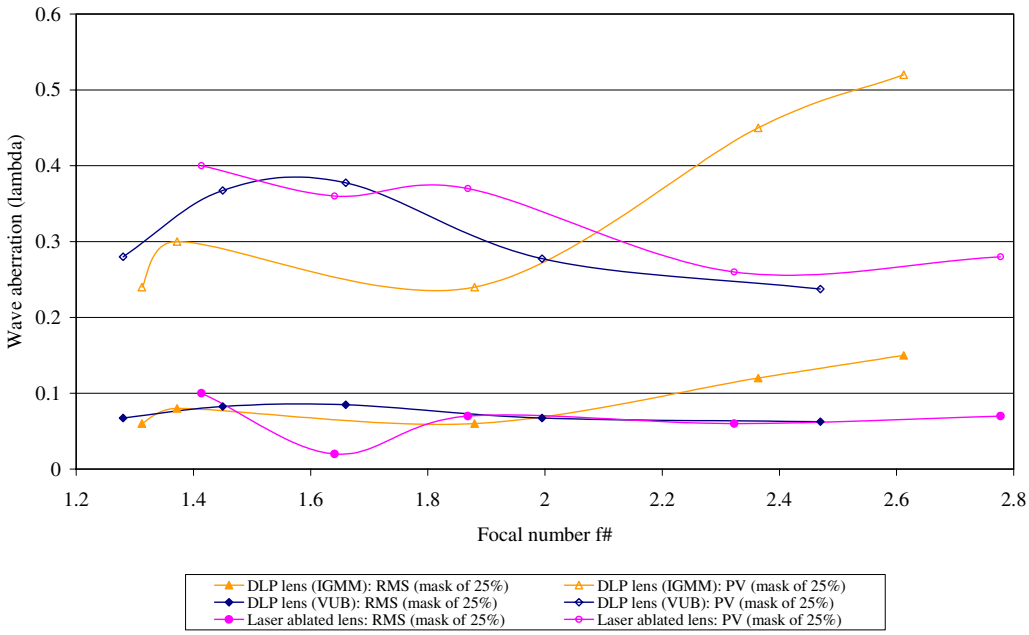

Figure 23. The RMS and PV wave aberrations (lambda) of both DLP microlenses (Institute of Geology, Mining and Materials (IGMM) and VUB) and laser ablated microlenses as a function of the focal number $f\#$ for a mask size of 25% of the microlens diameter ($\lambda = 632.8$ nm).

spherical microlenses with an index of refraction of 1.48. For microlenses fabricated with ion exchange, thermal reflow, reactive ion etching and direct laser writing we only obtained arrays of microlenses featuring a single focal number. This means that we only know their optical quality for one f-number ($f\#$). Therefore, we did not include their results in figures 20 and 21. As the RMS and PV aberrations change in a similar way as a function of the $f\#$, we discuss them simultaneously by speaking of 'wavefront aberrations'.

For microlenses obtained with deep lithography with protons we can compare the results from two different research groups (VUB and Institute of Geology, Mining and Materials). Because these microlenses are determined by the effect of surface tension we expect that for a given diameter of the lens there will be only one focal length and thus one focal number f for which the aberrations are minimized. For the microlenses fabricated at the VUB we observe as expected that the aberrations decrease with an increase of the $f\#$.

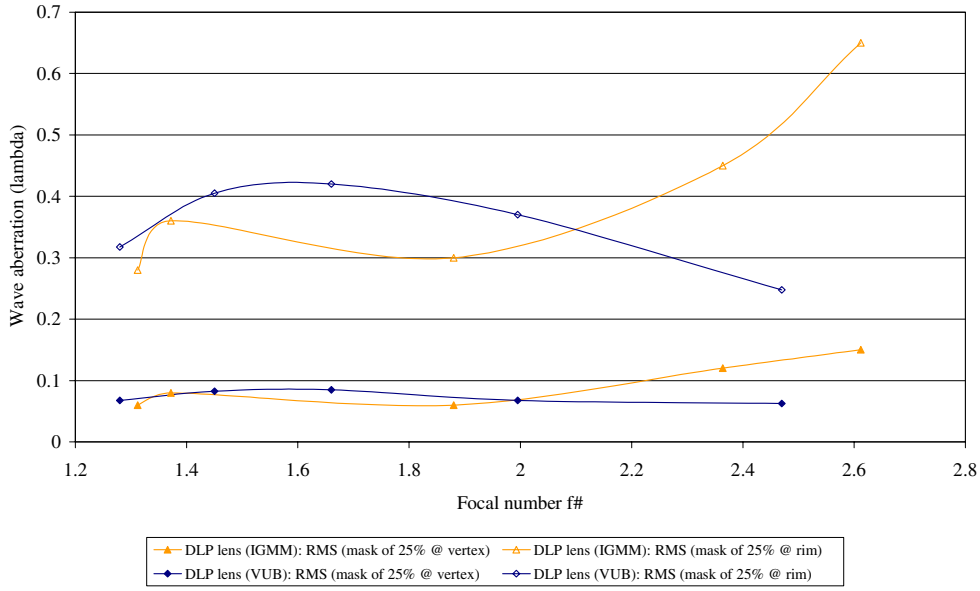

Figure 24. The RMS and PV wave aberrations (lambda) of both DLP microlenses (Institute of Geology, Mining and Materials (IGMM) and VUB) as a function of the focal number $f\#$ for a mask size of 25% of the microlens diameter (= mask of 25% @ vertex) and for the outer 25% of the lens diameter (= mask of 25% @ rim) ($\lambda = 632.8$ nm).

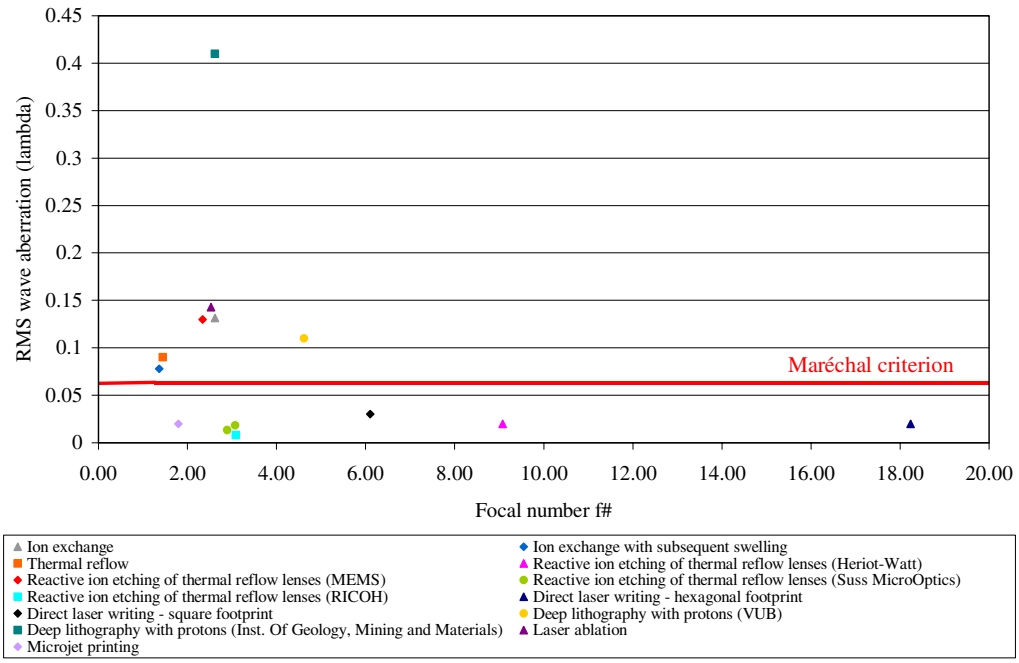

Figure 25. RMS wave aberrations (lambda) as a function of the focal number $f\#$ for the highest quality microlens of each fabrication technique ($\lambda = 632.8$ nm).

However, the experimental aberration values are higher than the theoretically predicted ones, mainly due to deviations from a perfect lens shape. For high $f\#$ s ($f\# > 5$) the aberrations tend to increase again. This latter increase is caused by a flattening of the lens curvature around the vertex.

For the microlenses from the Institute of Geology, Mining and Materials we see that for very low f numbers the aberrations are becoming higher for an increasing $f\#$. We also know that for lenses with a low $f\#$ the polymer material starts to flow beyond the targeted lens diameter during the swelling due to surface tension. This results in a non-spherical lens shape, decreasing the wavefront aberrations. Moreover, it is important to remark that for the microlenses made in the Institute of Geology, Mining and Materials we observe a similar behaviour as for the lenses of the VUB but the second aberration increase occurs at much lower $f\#$ ($f\# = 2$ as compared to $f\# = 5$), resulting in a lower focal length for which the optical performance is optimum. The reason for this

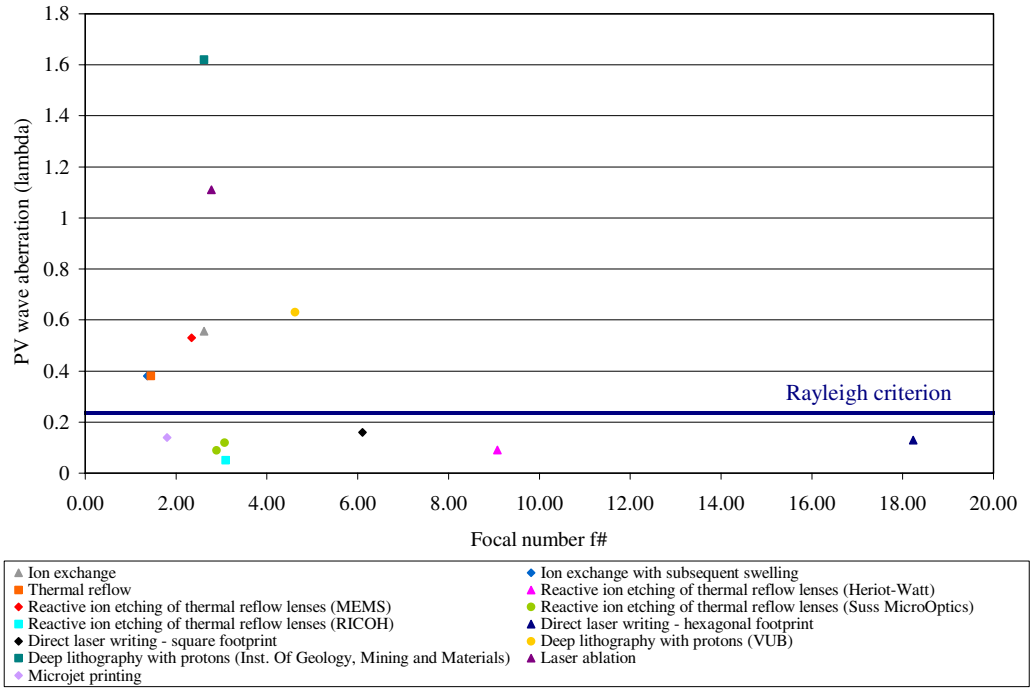

Figure 26. PV wave aberrations (lambda) as a function of the focal number $f\#$ for the highest quality microlens of each fabrication technique ($\lambda = 632.8$ nm).

Table 4. The RMS and PV wave aberrations (lambda) of DLP microlenses (VUB) for different focal numbers $f\#$ and for mask sizes of 25% and 100% of the microlens diameter.

$f\#$	DLP (25% mask)	DLP (100% mask)
RMS wavefront aberration		
1.31	0.06	1.31
1.37	0.08	1.37
1.88	0.06	1.88
2.36	0.12	2.36
2.61	0.15	2.61
PV wavefront aberration		
1.31	0.24	1.68
1.37	0.3	1.926
1.88	0.24	1.42
2.36	0.45	2.62
2.61	0.52	2.69

is that above this focal number the vertex area starts to become flat, resulting in an increase of the aberrations.

The last microlens fabrication technique displayed in figures 20 and 21 is microjet printing. These microlenses are also obtained by the effect of surface tension, which means that we also can expect the lowest aberrations at one particular (optimum) focal length for each lens diameter. The curve shows the aberrations of 700 μm diameter microjet printed lenses as a function of the focal number $f\#$. From these measurements we observe that the aberrations decrease from the lowest focal number on and that only a few focal lengths are diffraction limited. For focal numbers higher than 1.8 we observe that the aberrations increase again. This is due to an insufficient number of polymer drops, resulting in a lens with a non-circular rim or a non-spherical shape. Moreover, we have to mention that for an $f\#$ of 1.8 the simulated aberrations are higher than the measured values. The reason is that higher NA microlenses feature higher spherical aberration, resulting in a blur or a defocalization in the image plane. In practice however, we measure smaller wave aberrations due to a relatively high deviation from a perfect sphere. This explains why for the microjet printed microlens the measured aberrations as compared to the simulated ones are lower. To fabricate other lens diameters, the diameters of the circular wetting footprint should be changed and the number of polymer droplets should be adapted to obtain the desired lens characteristics. In practice it should be further investigated if diffraction-limited optical performance can be obtained for other $f\#$s.

In figures 20 and 21 we did not include the laser ablated microlenses because we could not measure the RMS and PV aberrations for 100% of the microlens diameter as they were way out of scale. It is however possible, by using the variable mask size feature of the Mach–Zehnder interferometer software, to quantitatively measure these aberrations over a limited part of the lens aperture. To investigate how the quality of the microlens decreases with increasing lens aperture we have plotted in figure 22 both the RMS and PV wave aberrations of a 200 μm diameter microlens with a focal length of 1283 μm and for mask sizes ranging between 8 and 52% of the lens diameter. As expected, we see that for higher mask sizes we find higher aberrations. Indeed, an aberration measurement in the vertex area shows a much better optical quality than if the whole lens area had been measured because the rim region has a high contribution to the overall aberration. Besides the results for the laser ablated microlens we plotted in figure 22 the RMS and PV wave aberrations as a function of the mask size for a 200 μm diameter lens with an identical focal length but this time fabricated with DLP (VUB). We can conclude that the aberration values are identical for a mask

Microlens fabrication technology	Wavefront aberration	MTF	PSF	Strehl ratio	Deviation from an ideal sphere	Surface roughness R_q (50 x 50 µm^2)	Ratio surface roughness / sag
Ion exchange D= 239.9 µm f= 627 µm f#= 2.62 NA= 0.19	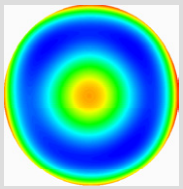 RMS 0.13 λ PV 0.56 λ	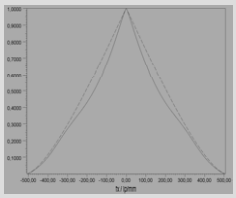	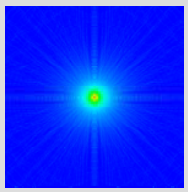	0.49			
Ion exchange with subsequent swelling D= 84.4 µm h= 6.8 µm f= 114.9 µm f#= 1.36 NA= 0.36	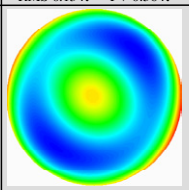 RMS 0.08 λ PV 0.38 λ	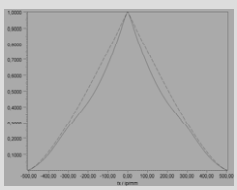	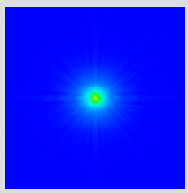	0.78		6.67 nm	0.09 %
Thermal reflow D= 144.7 µm h= 20.2 µm f= 209 µm f#= 1.44 NA= 0.3445	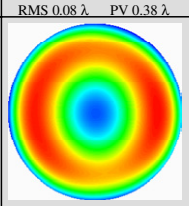 RMS 0.09 λ PV 0.38 λ	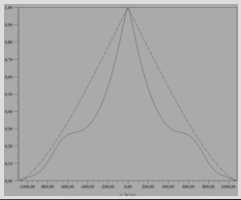	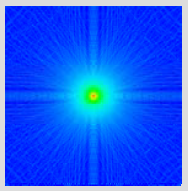	0.7036	RMS 0.0936 λ PV 0.5753 λ	1.87 nm	0.01 %
Reactive ion etching (Heriot-Watt) D= 199.3 µm h= 5.7 µm f= 1809 µm f#= 9.19 NA= 0.0544	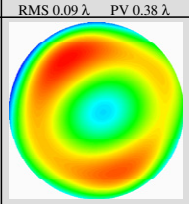 RMS 0.02 λ PV 0.09 λ	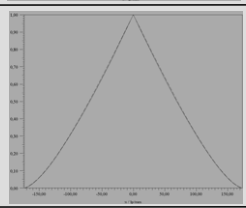	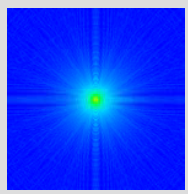	0.9894	RMS 0.1051 λ PV 0.4425 λ	1.55 nm	0.03 %
Reactive ion etching (McGill – MEMS Opt.) D= 117 µm h= 13.76 µm f= 274 µm f#= 2.38 NA= 0.21	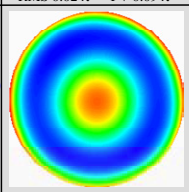 RMS 0.13 λ PV 0.53 λ	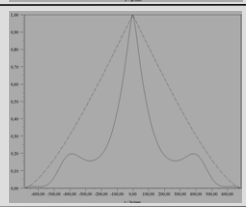	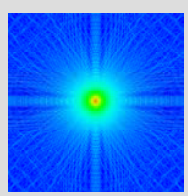	0.4866	RMS 0.1120 λ PV 0.7019 λ	1.97 nm	0.01 %
Reactive ion etching (Suss MicroOptics) D= 234.2 µm h= 22.2 µm f= 676.6 µm f#= 2.89 NA= 0.1765	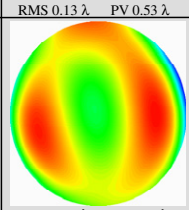 RMS 0.01 λ PV 0.09 λ	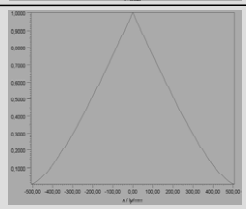	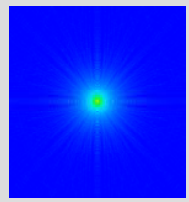	0.99		1.34 nm	0.01 %

Figure 27. Overview of the geometrical characteristics (diameter, sag, surface roughness and deviation from a perfect sphere) and optical lens characteristics (focal length, $f\#$, NA, wavefront aberration, MTF, PSF and Strehl ratio) for the different microlens fabrication techniques ($\lambda = 632.8$ nm) * The RMS surface roughness of this microlens is evaluated in a vertex area of 20×20 μm^2.

size lower than 40% of the lens diameter. Larger mask sizes however show that for laser ablated lenses the PV aberrations increase faster and go off scale beyond 52%.

To further evaluate the measurement results obtained on the laser ablated microlenses we have shown in figure 23 the RMS and PV wavefront aberrations for laser ablated microlenses and both types of DLP microlenses (Institute of Geology, Mining and Materials (IGMM) and VUB). We observe that for an identical mask size, i.e. 25% of the lens diameter, the RMS aberrations of the various types of microlenses are comparable. Only for DLP microlenses from the IGMM do we observe an increase in aberration for focal numbers higher than 1.8. An analogous behaviour can be found for the rim region of these lenses (see figure 24). For the VUB DLP lenses we can conclude that the aberrations in the vertex area are constant and independent of the focal number. However, as shown in figure 24 the rim region of these lenses contributes more to the wave aberrations and decreases for an increasing focal number, except for focal numbers $f\#$ lower than 1.6 where the lens shape is aspherical. The higher PV aberration for both types of DLP lenses can be ascribed to local defects on the microlens (e.g. a non-perfect mask aperture; small dust particles on the microlens surface). When we now

Microlens fabrication technology	Wavefront aberration	MTF	PSF	Strehl ratio	Deviation from an ideal sphere	Surface roughness R_q (50 x 50 µm²)	Ratio surface roughness / sag
Reactive ion etching (RICOH Company) D= 38 µm h= 3.52 µm f= 117.5 µm f#= 3.09 NA= 0.16	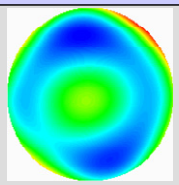 RMS 0.01 λ PV 0.05 λ	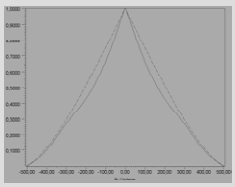	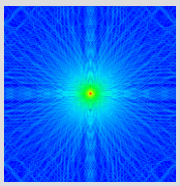	0.99		2.89 nm*	0.08 %
Direct laser writing D= 219.3 µm h= 1.67 µm f= 3999 µm f#= 18.32 NA= 0.0273	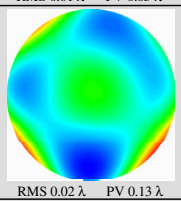 RMS 0.02 λ PV 0.13 λ	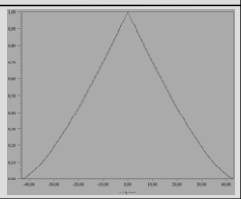	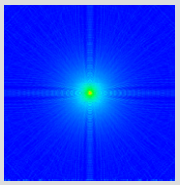	0.9853	RMS 0.0975 λ PV 0.9277 λ	28.65 nm	1.72 %
DLP (Inst. Of Geology, Mining and Materials D= 173.3 µm h= 15.2 µm f= 454 µm f#= 2.64 NA= 0.1894	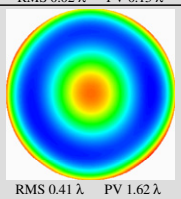 RMS 0.41 λ PV 1.62 λ	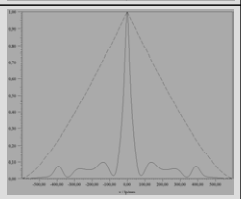	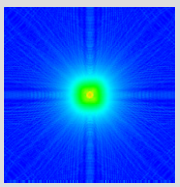	0.12		2.71 nm	0.02 %
DLP (VUB) D= 197.4 µm h= 11.5 µm f= 912 µm f#= 4.62 NA= 0.1082	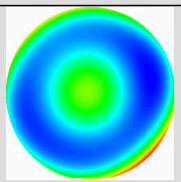 RMS 0.11 λ PV 0.63 λ	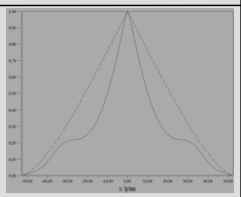	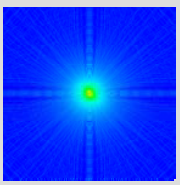	0.6293		2.14 nm	0.01 %
Laser ablation D= 199.8 µm h= 16.38 µm f= 555.45 µm f#= 2.85 NA= 0.1755	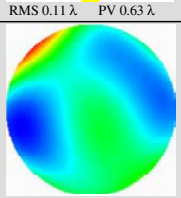 RMS 0.16 λ PV 1.11 λ	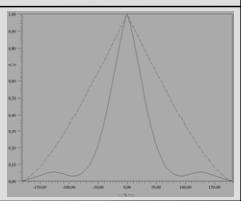	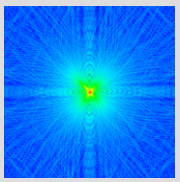	0.4028		3.14 nm	0.02 %
Microjet printing D= 687.1 µm h= 98.2 µm f= 1235 µm f#= 1.91 NA= 0.2619	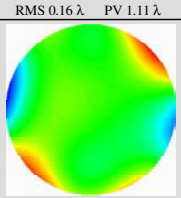 RMS 0.02 λ PV 0.14 λ	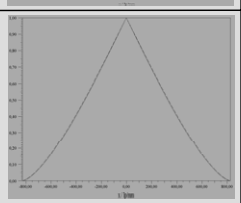	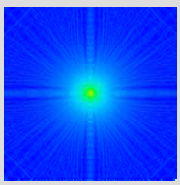	0.9898	RMS 0.2715 λ PV 1.5880 λ	3.03 nm	0.01 %

Figure 27. (Continued.)

compare the results for a mask size of 25% and 100% of the DLP lens diameter we observe a tremendous deterioration of the microlens performance when using mask sizes above 25% of the lens diameter (see table 4). This conclusion is also very important when interpreting the optical performance of the 200 μm laser ablated microlenses. Indeed, we cannot come to a decisive conclusion as these microlenses cannot be measured with a mask size beyond 55%.

In figure 25 we have summarized the RMS wave aberrations of the highest quality microlens for each of the different fabrication techniques as a function of the focal number. We included the measurement results of both those microlenses of which we only characterized one set of parameters, and of those of which we investigated a range of focal numbers. From these measurements we can conclude that only the microlenses fabricated with microjet printing (MicroFab Inc.), laser beam writing (Heptagon), reactive ion etching (Heriot–Watt University, Suss MicroOptics and RICOH Company) and ion exchange with subsequent swelling (NSG) are diffraction limited according to the Maréchal criterion ($\psi_{\mathrm{RMS}} \leqslant \lambda/14$). We can remark that the studied thermal reflow microlenses are not diffraction limited due to their low $f\#$, although increasing the $f\#$ will lower the aberrations. However, there is a limitation because when microlenses are fabricated by the effect of surface tension slow lenses (long focal length or high $f\#$) tend to flatten in the vertex area. The same remarks can be made for thermal reflow microlenses transferred in fused silica via reactive ion etching (MEMS Optical). Along the same lines we observe in figure 26 that all the microlenses for which the Maréchal criterion is

Table 5. Measured and simulated RMS and PV wave aberrations (lambda) and their ratios as well as the Strehl ratio.

	Measured RMS aberration (λ)	Simulated RMS aberration (λ)	Ratio Meas./sim. RMS aberration (λ)	Measured PV aberration (λ)	Simulated PV aberration (λ)	Ratio Meas./sim. PV aberration (λ)	Measured Strehl ratio	Simulated Strehl ratio	Ratio Meas./sim. Strehl ratio
Deep lithography with protons (Inst. of Geology, Mining and Materials)	0.41	0.0174	23.6	1.62	0.0652	24.8	0.12	0.9698	0.1
Deep lithography with protons (VUB)	0.11	0.0039	28.2	0.63	0.0146	43.0	0.63	0.9991	0.6
Direct laser writing—hexagonal footprint	0.02	0.0008	25.6	0.13	0.0003	445.2	0.99	1.0000	1.0[b]
Laser ablation	0.16	0.0122	13.1	1.11	0.0456	24.3	0.40	0.9882	0.4
Microjet printing	0.02	0.0485	0.4[a]	0.14	0.1817	0.8[a]	0.99	0.8039	1.2[b]
Photothermal technique + ion exchange	0.17	0.0471	3.6[a]	0.95	0.1770	5.4[a]	0.34	0.8107	0.4
Reactive ion etching of thermal reflow lenses (Heriot–Watt)	0.02	0.0006	32.5	0.09	0.0023	39.1	0.99	1.0000	1.0[b]
Reactive ion etching of thermal reflow lenses (MEMS optical)	0.13	0.0175	7.4	0.53	0.0655	8.1	0.49	0.9537	0.5
Reactive ion etching of thermal reflow lenses (RICOH Company)	0.01	0.0028	3.6[a]	0.05	0.0104	4.8[a]	0.99	0.9993	1.0[b]
Reactive ion etching of thermal reflow lenses (Suss MicroOptics)	0.01	0.0065	1.5[a]	0.09	0.0243	3.7[a]	0.99	0.9973	1.0[b]
Thermal reflow	0.09	0.0333	2.7[a]	0.38	0.1226	3.1[a]	0.70	0.7748	0.9[b]

[a] Appropriate for imaging applications.
[b] Suitable for light collection applications.

fulfilled also show a diffraction-limited optical performance according to the Rayleigh criterion ($\psi_{PV} \leqslant \lambda/4$).

As an overview we list in figure 27 for the highest quality microlens of each technology both the geometrical characteristics (namely the diameter D, the sag h and the ratio of the surface roughness/sag) and the optical characteristics (namely the focal length f, the focal number $f\#$, the numerical aperture NA, the RMS and PV wave aberrations, the MTF, the PSF, the Strehl ratio and the deviation from a perfect sphere).

As we mentioned earlier, it is difficult if not impossible to further compare the characteristics of the different microlenses because of the difference in the various relevant parameters like their diameters and focal lengths. As known, the wave aberrations are decreasing for an increasing focal length when the diameter is chosen constant and the aberrations are increasing for an increasing diameter at a fixed focal length. Because we have here a wide range of diameters and focal lengths we compare the optical characteristics obtained through measurements with values obtained through ray-trace modelling of perfect spherical microlenses with identical sag, diameter and radius of curvature. In table 5 we summarize for the RMS and PV aberrations and for the Strehl ratio the deviation of the measured value as compared to the simulated one for the various refractive microlens techniques. The microlenses fabricated with ion exchange and with ion exchange and a subsequent swelling are not included in this comparison as we were not able to obtain the index distribution in the microlens for modelling purposes. We can conclude that for imaging applications where diffraction-limited performance is a quintessential requirement, microjet printing, thermal reflow and reactive ion etching (RICOH and Suss MicroOptics) are the most developed and optimized technologies. Microlenses, made with reactive ion etching of thermal reflow microlenses (MEMS Optical) or with laser ablation, need some further improvement before they can be applied in imaging applications.

Furthermore, we observe that the ratios between the measured and simulated values for the RMS and the PV aberrations behave similarly, except for the laser beam written lenses, where there exists a large difference in PV aberration between the measured and the simulated value. This may be due to the high RMS surface roughness of these microlenses and can cause problems in applications where background noise and cross talk are critical issues. In applications where not the imaging quality but the maximum collection of light is most essential, the Strehl ratio has to be higher than 0.8. This requirement is fulfilled for microlenses fabricated with direct laser beam writing, microjet printing and thermal reflow combined with reactive ion etching (by Heriot–Watt University, RICOH and Suss MicroOptics). Microlenses made

Table 6. Overview of the most important refractive microlens fabrication techniques: geometrical and optical parameters, material selection, replication possibility, fabrication time (for a 10 × 10 array) and the possibility for monolithic integration. (Note: bold characters represent measurement results and others represent the literature; own)

	D (μm)	f (μm)	f#	NA	SA (λ)	Strehl ratio	Fill factor	Material	Replication (in plastics)	Fabrication time	Monolithic integration	Ref.
Surface relief lenses (polymer)												
Thermal reflow												
No base layer	5–750		0.8–2	0.2–0.56				Photoresist	Yes	Parallel process	—	[33]
No base layer	5–750	70–1300	1–2.5	0.2–0.5	0.663	0.75		Photoresist	Yes	Parallel process	—	[54]
Base layer	10–200			0.3–0.5				Photoresist	Yes	Parallel process	—	[9]
Base layer	150–400			0.1–0.3	0.11			Photoresist	Yes	Parallel process	—	[34]
	10–2000		1–15					Photoresist	Yes	Parallel process	—	[54]
	145	**201.9–211.3**		**0.29–0.34**	**0.11–0.12**	**0.58–0.62**	**83%**	**Photoresist**	**Yes**	**Parallel process**	**—**	**Exp. data**
Direct laser beam writing	10–100 00	200–6000			<0.04		Near 100%	Photoresist or polymer on glass	Yes	Sequential process	Hybrid microlenses	[37, 39]
	30/129	**176.5/3893**		**0.08/0.03**	**0.04/0.02**	**0.94/0.97**						**Exp. data**
Deep lithography with protons	5–1800	166–1444	0.83–7.22		<0.21		<80%	PMMA	Yes	Sequential process (10 min +3 h)[a]	Beam-splitter, microprisms, fibre-holder, mechanical alignment features	[10, 43]
	125–250	**143–912**	**0.7–5**	**0.1–0.7**	**0.01–0.6**							**Exp. data**
Hydrophobic effect	2–500		1.38–12				<90%	UV curable monomer on Si, SiO_2, SiN, GaAs, InGaAs and InP	Yes	Parallel process	Directly on optical fibres	[55, 56]
Laser ablation	50–385	100–650		0.2–0.3			<50%	PMMA, PS, PC	Yes	Sequential process (4 h)[a]	—	[14]
	200	**194–1283**		**0.07–0.52**	**0.08–0.23**	**0.1–0.4**						**Exp. data**
Microjet printing	20–5000		0.9–30		<0.6		<90%	UV curing optical expoxy	Yes	Sequential process (10 min)	Directly on optical substrates and components (fibres, waveguides, CSELs)	[50, 51]
	50–2000	100–10 000						Solgel l	Yes	Sequential process		[57]
	700	**844–1420**		**0.12–0.26**	**0.02–1.48**	**0.04–0.09**						**Exp. data**
GRIN microlenses (glass)												
GRIN rod	>1000		0.7–5	0.1–06				Glass	No		—	[29]
Planar microlens											—	
Ion exchange	10–1000	20–4000		0.02–0.25	3.429	0.05		Glass, plastics	No	Parallel process		[29, 30]
	240	**627**		**0.19**	**0.3**	**0.46**						**Exp. data**
Ion exchange with swelled structure	10–400			<0.57				Glass	No	Parallel process		[30]
	85	**115**		**0.36**	**0.16**	**0.77**						Exp. data

with deep lithography with Protons (VUB) and with reactive ion etching (MEMS Optical) have to be further optimized to enhance the Strehl ratio to the minimum value of 0.8.

Although our study comprises the most important microlens fabrication techniques, it is incomplete for three reasons: firstly because some fabrication techniques are missing, secondly because in a few cases we were not able to study the top-quality microlenses, and thirdly because most of the microlenses we have been provided with do not cover the entire parameter range, but only a limited number

Table 6. (Continued.)

	D (μm)	f (μm)	f#	NA	SA (λ)	Strehl ratio	Fill factor	Material	Replication (in plastics)	Fabrication time	Monolithic integration	Reference
Surface relief lenses (glass)												
Photothermal technique	70–1000		0.8–2	<0.35				Photosensitive glass	Yes	Parallel process (1 h)	—	[3, 29]
Photothermal technique + ion exchange	500–1250	1274–19 201		0.03–0.20	0.17–0.85	0.02–0.34						[3, 29]
CO_2 irradiation	50–800			<0.4				Glass	Yes	Sequential process	—	[5]
Visible laser irradiation	15–150		1–2.5		0.08			Borosilicate doped glass	Yes	Sequential process	—	[58]
Reactive ion etching of thermal rerflow microlenses	150–400							Fused silica, Si, InP, GaAs	—	Parallel process (1 h)		[59, 60]
	200	**1818–1955**		**0.05**	**0.03**	**0.97**	**90%**					**Exp. data**
	123	**282**		**0.21**	**0.15**	**0.4**	**75%**					**Exp. data**
	245	**750**		**0.16**	**0.03**	**0.99**						**Exp. data**
	10–40	**30–120**		**0.16–0.31**	**0.006–0.04**	**0.99**	**50%**					**Exp. data**

[a] It is also possible with this fabrication technique to expose a mask with an array of holes to reduce the fabrication time of the microlenses. In that case we have a parallel process. Sometimes however this approach will limit the variety of characteristics a microlens array can harbour.

of different diameters and sags. We therefore suggest to fabricate with each of the discussed technologies the same set of microlenses, such that a more complete comparison becomes possible. We also propose that this set of microlenses should cover a wide range of focal numbers ranging from 1 to 15, corresponding to NAs from 0.50 to 0.03. By choosing a wide range of microlens parameters we can determine for each of the microlens fabrication techniques the range in which spherical microlenses can be made. Additionally, we can investigate the reproducibility of the fabrication process and we can test whether the targeted specifications can be achieved. Meanwhile, we can conclude that although some research groups or companies claim that they fabricate high-quality optical microlenses they seldom are able to support this claim with quantitative specifications. As a matter of fact, our in-depth study shows that very high-quality microlenses are rather the exception than the rule. We would therefore like to open a pleading for setting up clear criteria for a microlens quality label.

Although we were not able to fully compare the performances of all the microlens fabrication methods, we have been able to assess the trends in performance for each technology. To complete our quantitative comparison on the parameter range of the different microlens fabrication techniques we have made a literature survey and summarized our findings in table 6. In this table we discuss for each of the fabrication techniques the range of geometrical and optical characteristics, the range of materials in which they can be produced, the feasibility of replicating the microlenses, the difference between a sequential and a parallel writing process, with in some cases an estimate of the fabrication time at the prototyping level, and the possibility of monolithic integration with other micro-optical components. The mentioned fill factor, important for light efficiency applications, is not necessarily the highest value which can be obtained with a certain fabrication technology. The numbers given in the table are experimentally determined from the delivered microlens samples. In general, we can say that thermal reflow, reactive ion etching, microjet printing and direct laser writing can deliver fill factors higher than 90%. All information in the table has to be used with caution because the published results may reflect 'lucky shots' or 'best results' rather than 'typical' lens characteristics.

4. Conclusions

In this paper we have reviewed the most important microlens fabrication techniques and we have quantitatively characterized the resulting microlenses which we obtained from selected research groups. All the quantitative results were obtained with a non-contact optical profiler, a transmission Mach–Zehnder interferometer and a Twyman–Green interferometer. We have studied the different technologies by comparing the geometrical and optical characteristics of the microlenses and by briefly touching upon the range of materials in which the lenses can be fabricated, their potential for low-cost fabrication through mass-replication techniques and for monolithic integration with other micro-optical components. We can conclude that a variety of techniques is nowadays available for the manufacturing of microlenses, although high-quality microlenses are still rather the exception than the rule. Some of these technologies like microjet printing and thermal reflow have been developed to a stage where it is now routine to make lenses of high optical imaging quality. Other techniques, such as reactive ion etching and direct laser writing, are well suited for the fabrication of microlenses for light collection applications. Still other technologies, like deep lithography

with protons and laser ablation, whose unique added value can be found in monolithic integration of microlenses with other micro-optical components or post-processing respectively, require some more refinement before they can be applied in a reliable way in commercial products.

Acknowledgments

This research is made possible through the financial support of the Fund for Scientific Research—Flanders (FWO-Vlaanderen), the IAP Photon Network, the Institute for the Promotion of Innovation by Science and Technology in Flanders (IWT), the IWT GBOU project 'Generic technologies for plastic photonics', the Research Council (OZR) of the Vrije Universiteit Brussel and the European Commission NoE 'NEMO'. Finally, the authors would like to thank Professor A Kirk from the McGill University and Professor K Hamanaka from Nippon Sheet Glass (NSG) for providing respectively microlenses from MEMS Optical and ion exchange microlenses.

References

[1] Sinzinger S and Jahns J 1999 *Microoptics* (New York: Wiley–VCH)
[2] Borrelli N F 1999 Part I: Optics and fabrication *Microoptics Technology: Fabrication and Applications of Lens Arrays and Devices* (New York: Dekker)
[3] Borrelli N F, Morse D L, Bellman R H and Morgan W L 1985 Photolytic technique for producing microlenses in photosensitive glass *Appl. Opt.* **24** 2520–5
[4] Oikawa M, Iga K, Sanada T, Yamamoto N and Nishizawa K 1981 Array of distributed-index planar microlens prepared from ion-exchange technique *Japan. J. Appl. Phys.* **20** L296–8
[5] Wakaki M, Komachi Y and Kanai G 1998 Microlenses and microlens arrays formed on a glass plate by use of a CO_2 laser *Appl. Opt.* **37** 627–31
[6] Gale M T 1997 *Replication, Micro-optics: Elements, Systems and Applications* ed H P Herzig (London: Taylor and Francis) chapter 6
[7] Keyes D L, Lamonte R R, McNally D and Bitritto M 2001 Polymers for photonics *Photonics Spectra* **35** (10)
[8] Popovic Z D, Sprague R A and Neville Connell G A 1988 Technique for monolithic fabrication of microlens arrays *Appl. Opt.* **27** 1281–4
[9] Jay T R *et al* 1994 Preshaping photoresist for refractive microlens fabrication *Opt. Eng.* **33** 3552–5
[10] Ottevaere H, Volckaerts B, Lamprecht J, Schwider J, Hermanne A, Veretennicoff I and Thienpont H 2002 2D plastic microlens arrays by deep lithography with protons: fabrication and characterization *J. Opt. A: Pure Appl. Opt.* **4** S22–8
[11] Ossmann C, Göttert J, Ilie M, Mohr J and Ruther P 1997 *Proc. Microlens Arrays EOS Topical Mtg* pp 54–8
[12] Croutxé-Barghorn C, Soppera O and Lougnot D J 2001 Fabrication of refractive microlens arrays by visible irradiation of acrylic monomers: influence of photonic parameters *Eur. Phys. J.: Appl. Phys.* **13** 31–7
[13] MacFarlane D L, Narayan V, Cox W R, Chen T and Hayes D J 1994 Microjet fabrication of microlens arrays *IEEE PTL* **6** 1112–4
[14] Naessens K, Ottevaere H, Baets R, Van Daele P and Thienpont H 2003 Direct writing of microlenses in polycarbonate with excimer laser ablation *Appl. Opt.* **42** 6349–59
[15] Gale M T 1997 Direct writing of continuous relief micro-optics *Micro-optics: Elements, Systems and Applications* ed H P Herzig (London: Taylor and Francis) chapter 4
[16] Kley E B, Possner T and Göring R 1993 Realization of micro-optics and integrated optic components by electron-beam lithographic surface profiling and ion exchange in glass *Int. J. Optoelectron.* **8** 513–27
[17] Khanarian G and Celanese H 2001 Optical properties of cyclic olefin copolymers *Opt. Eng.* **40** 1024–9
[18] Beich W S 2002 Specifying injection-molded plastic optics *Photonics Spectra* **40**
[19] Pedrotti F L and Pedrotti L S 1993 Optical instrumention *Introduction to Optics* 2nd edn (Englewood Cliffs, NJ: Prentice-Hall) chapter 6
[20] Savage N 2002 The future is plastics *SPIE's OE Magazine* p 44
[21] http://www.gsoptics.com
[22] http://www.sunex.com/doc/whitpap.pdf
[23] Ottevaere H and Thienpont H 2004 Refractive optical microlenses: an introduction to nomenclature and characterization techniques *Encyclopedia of Modern Optics* vol 4, ed R D Guenther, D G Steel and L Bayvel (Oxford: Elsevier) pp 21–43 (ISBN 0-12-227600-0)
[24] Oikawa M, Iga K and Sanada T 1981 A distributed-index planar microlens made of plastics *Japan. J. Appl. Phys.* **20** L51–4
[25] Moore D T 1980 Gradient-index optics: a review *Appl. Opt.* **19** (7)
[26] Bähr J, Krackhardt U and Brenner K H 2001 Fabrication and testing of planar microlens arrays by ion exchange technique in glass *Micro- and Nano-Optics For Optical Interconnection and Information Processing* (*Proc. SPIE* vol 4455) (Bellingham, WA: SPIE) pp 281–92
[27] Oikawa M, Iga K and Sanada T 1981 Distributed-index planar microlens array prepared from deep electromigration *Electron. Lett.* **17** 452–4
[28] http://www.nsgamerica.com/
[29] Hutley M C 1997 Refractive lenslet arrays *Micro-optics: Elements, Systems and Applications* ed H P Herzig (London: Taylor and Francis) chapter 5
[30] Oikawa M, Nemoto H, Hamanaka K and Okuda E 1990 High numerical aperture planar microlens with swelled structure *Appl. Opt.* **29** 4077–80
[31] Bähr J, Brenner K H, Sinzinger S, Spick T and Testorf M 1994 Index-distributed planar microlenses for three-dimensional micro-optics fabricated by silver–sodium ion exchange in BGG35 substrates *Appl. Opt.* **33** 5919–24
[32] Hutley M C 1990 Optical techniques for the generation of microlens arrays *J. Mod. Opt.* **37** 253–65
[33] Daly D, Stevens R F, Hutley M C and Davies N 1990 The manufacture of microlenses by melting photoresist *Meas. Sci. Technol.* **1** 759–66
[34] Haselbeck S, Schreiber H, Schwider J and Streibl N 1993 Microlenses fabricated by melting a photoresist on a base layer *Opt. Eng.* **32** 1322–4
[35] Nussbaum P H, Völkel R, Herzig H P, Eisner M and Haselbeck S 1997 Design, fabrication and testing of microlens arrays for sensors and microsystems *Pure Appl. Opt.* **6** 617–36
[36] Stern M B and Jay T R 1994 Dry etching for coherent refractive microlens arrays *Opt. Eng.* **33** 3547–51
[37] Harriott L R, Scott R E, Cummings K D and Ambrose A F 1986 Micromachining of integrated optical structures *Appl. Phys. Lett.* **48** 1704–6
[38] Harder I, Lindlein N and Schwider J 2001 Fabrication of microlens arrays with the help of greytone lithography and RIE *Annual Report Lehrstuhl für Optik* p 28
[39] http://www.heptagon.fi/products
[40] Volckaerts B, Ottevaere H, Vynck P, Debaes C, Tuteleers P, Hermanne A, Veretennicoff I and Thienpont H 2001 Deep lithography with protons: a generic fabrication technology for refractive micro-optical components and modules *Asian J. Phys.* **10** 195–214
[41] Brenner K-H, Frank M, Kufner M and Kufner S 1990 H+-Lithography for 3-D integration of optical circuits *Appl. Opt.* **29** 3723–4

[42] Woo H-J, Kim Y-S, Choi H-W, Hong W, Lee S, Kufner M and Kufner S 2001 Optimisation of microlenses fabricated by deep proton irradiation and styrene diffusion *Microelectron. Eng.* **57/58** 945–51

[43] Optoelectronic interconnects for integrated circuits (1996–2001), Advanced research initiative in microelectronics MEL-ARI OPTO http://www.intec.rug.ac.be/oiic/

[44] Schmidt H 1994 Automated excimer laser carves microstructures *Opt. Laser Eur.* (9) 35–7

[45] Mihailov S and Lazare S 1993 Fabrication of refractive microlens arrays by excimer laser ablation of amorphous Teflon *Appl. Opt.* **32** 6211–8

[46] Beinhorn F, Ihlemann J, Luther K and Troe J 1999 Microlens arrays generated by UV laser irradiation of doped PMMA *Appl. Phys.* A **68** 709–13

[47] Matz R, Weber H and Weimann G 1997 Laser-induced dry etching of integrated InP microlenses *Appl. Phys.* A **65** 349–53

[48] Naessens K, Van Daele P and Baets R 2001 Laser ablation based technique for flexible fabrication of microlenses in polymer materials *Proc. 2nd Int. Symp. on Laser Precision Microfabrication (Singapore)* pp 124–7

[49] Naessens K, Van Daele P and Baets R 2000 Microlens fabrication in PMMA with scanning excimer laser ablation techniques *Proc. 5th Annual Symp. IEEE/LEOS Benelux Chapter (Delft, Netherlands)* pp 99–102

[50] Chen T, Cox W R, Lenhard D and Hayes D J 2002 Microjet printing of high precision microlens array for packaging of fiber-optic components *SPIE Proc. Photonics Packaging and Integration IV* vol 4652 (Bellingham, WA: SPIE) pp 136–41

[51] Keyworth B P, Corazza D J, McMullin J N and Mabbott L 1997 Single-step fabrication of refractive microlens arrays *Appl. Opt.* **36** 2198–202

[52] Cox W R, Chen T and Hayes D J 2001 Micro-optics fabrication by inkjet printing *Opt. Photon. News* **12** 32–5

[53] Cox W R, Guan C and Hayes D J 2000 Microjet Printing of micro-optical interconnects and sensors *Proc. SPIE Photonics (West, San Jose)* vol 3852 (Bellingham, WA: SPIE) pp 400–8

[54] Hutley M C 1991 Microlens arrays *Phys. World* **4** 27–32

[55] Hartmann D M, Kibar O and Esener S C 2000 Characterization of a polymer microlens fabricated by use of the hydrophobic effect *Opt. Lett.* **25** 975–7

[56] Hartmann D M, Reiley D J and Esener S C 2001 Microlenses self-aligned to optical fibers fabricated using the hydrophobic effect *IEEE Photon. Technol. Lett.* **13** 1088–90

[57] http://www.solgel.com/labfoc/inm/micro_e.html

[58] Fritze M, Stern M B and Wyatt P W 1998 Laser-fabricated glass microlens arrays *Opt. Lett.* **23** 141–3

[59] Kufner M and Kufner S 1997 Conclusions *Micro-optics and Lithography* (Brussels: VUB Press) chapter 11

[60] Eisner M and Schwider J 1996 Transferring resist microlenses into silicon by reactive ion etching *Opt. Eng.* **35** 2979–82